REVIEW ARTICLE - MECHANICAL ENGINEERING

A State-of-the-Art Review on Manufacturing and Additive Influences on Sand-Cast Components

Prafulla Kumar Sahoo[1] · Sarojrani Pattnaik[1] · Mihir Kumar Sutar[1]

Abstract

Sand casting is the one of the oldest fabrication techniques, which has a number of important technological challenges with respect to improving productivity and quality of the castings. It is essential for the foundries to reduce or eliminate the casting defects if they need to survive in this highly competitive global market. This review arises from a strong industrial demand for understanding the physical and process parameters to improve the quality and soundness of the sand-cast products. The present article primarily reviews the investigations done by researchers on the usability of locally available silica sands and clays for casting both ferrous and non-ferrous alloys. The paper highlights the application of artificial intelligence techniques in predicting the sand mould quality and further optimizing the casting process parameters. This article also analyses the potentials and feasibility of three-dimensional printing in sand casting process. Further, the role of different additives on sand mould composition and different trace elements or inoculants on mechanical properties and microstructure of sand casting has been discussed. Finally, elaborations have been made about various types of hybrid sand casting processes along with metal matrix composites.

Keywords Sand casting · Three-dimensional printing · Additives · Taguchi method · Defects

1 Introduction

Casting is one of the primitive methods to manufacture metallic components. As per Pio et al. [1], the first metal casting was produced at some point in 4000–3000 BC. Ever since, different casting methods have been evolved. The liquid material in the casting process is discharged into a hollow space known as mould or die, which corresponds to the needed shape and size of the component to be produced. Subsequently, the cast part is solidified and taken out from the hole as a solid component. A detailed explanation of the fundamental stages associated with the manufacture of a sand casting via sand mould, as depicted in Fig. 1, is given by Kalpakjian and Schmid [2]. As per their presentation, the process involves the insertion of a pattern inside the sand to create an impression, filling the resultant hollow space with melt, permitting the melt to chill before solidification, collapsing the sand mould, and ejecting the casting. Even if

their presentation includes only the basic steps and outlines the sand casting process, it aids a novice to understand the fundamentals of the process.

Sand casting is mostly used for high volume production where surface finish and dimensional accuracy are not critical. This process is suitable for casting any metal or alloy irrespective of any shape, size or load of the casting. The main disadvantage of the process is that it necessitates for machining operation with the purpose of getting good surface finish to the castings, especially large casting having rough surface texture. Figures 2 [3] and 3 [4] show different cast products using a sand mould.

Nowadays, simulation of sand casting process is widely employed because of its capability to give more reliable results in a relatively shorter time. The simulation of a model of the sand casting process is aimed at finding out the feasibility of the process so as to enhance the quality of the cast part. The developments that have taken place or taking place in sand casting are improved methods to construct the sand moulds, usage of better mould handling and melting equipment and automatic conditioning of sand, pouring of melt in moulds and shake out the operation. This review article throws light on improving the mechanical properties of sand

✉ Sarojrani Pattnaik
  sarojrani07@gmail.com

[1] Mechanical Engineering Department, Veer Surendra Sai University of Technology, Burla, Odisha 768018, India
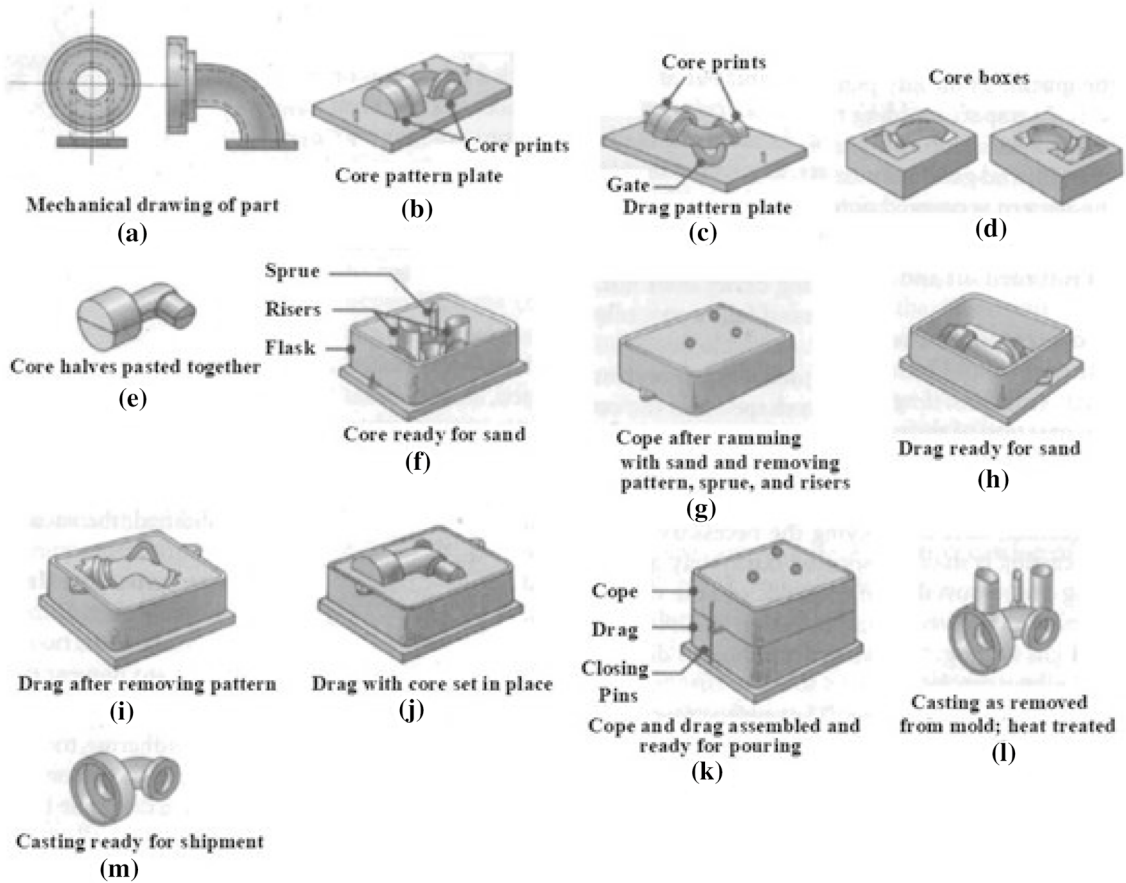
Fig. 1 Fundamental stages of sand casting process: **a** mechanical drawing of part; **b** core pattern plate; **c** drag pattern plate; **d** core boxes; **e** core halves pasted together; **f** cope ready for sand; **g** cope after ramming with sand and removing pattern, sprue and risers; **h** drag ready for sand; **i** drag after removing pattern; **j** drag with core set in place; **k** cope and drag united for pouring; **l** cast part as removed from mould; **m** casting ready for delivery [2]

Fig. 2 Gray iron casting using sand mould [3]

Fig. 3 Funnel using sand mould [4]

casting by improving the sand mould properties and using different processing conditions of the melt for casting.

2 Factors Influencing the Mechanical Properties and Permeability of Sand Mould

2.1 Effect of Different Constituents in Controlling Sand Mould Properties

The sand mould is made usually from silica sand (80%), clay binders (5–10%) mostly bentonite, tempering water (2–6%) and different additives. Moisture-containing moulding sand is known as green moulding sand. As per Kundu and Lahiri [5], the moulding sand mixture composition is very crucial in determining the sand mould properties. Sand mixture properties and behaviour depend upon the following factor: (1) the sand grain shape and size; (2) the content and nature of clays; (3) additives and moisture; (3) effectiveness of mulling the raw materials, etc. The moulding sand can be reused repeatedly. However, every recycling requires adding up of binder and water into the used moulding sand mixture. If the amount of binder and water is inaccurate, the sand mould's binding strength decreases. It would lead to a considerable decrease in the green sand mould properties and, consequently, augment the number of casting rejection rates.

The main constituent in building a green sand mould for casting both ferrous and non-ferrous alloys is the sand. Clay is added to bind the moulding sand mixture so that the mould gets enough strength for casting. Olasupo and Omotoyinbo [6] prepared sand moulds from locally available Nigerian silica–clay mixture and studied the mould properties such as strength, permeability and refractoriness for casting ferrous and non-ferrous parts. It was found that the blend of Igbokoda silica sand and Ijero-Ekiti clay possessed adequate strength, permeability and refractoriness as required for foundry applications. Ademoh [7] mixed bentonite or kaolin clay with the river Niger sand to study the moulding properties of the mixture. It was found that the bonding property of Kaolin clay was better than that of the bentonite clay. Further, the sand mould containing 1% kaolin clay, 2.5% bentonite clay and 2% moisture was found to be the best combination for casting non-ferrous alloys.

Lanre and Olumodeji [8] explored the foundry properties, namely green compression strength (GCS), shatter index and permeability of Ilorin sand for casting both non-ferrous and ferrous alloys. The GCS value was found to lie between 36 and 60 KN/m^2. The range of shatter index and permeability values was from 31 to 84 and from 47 to 68.3, respectively. Fo et al. [9] prepared the sand mould from Onitsha beach Niger River sand and Ukpor clay to study the important mould properties (green compression strength, dry compression strength (DCS) and permeability). It was established by them that the GCS and DCS of the sand mould augmented amazingly when the Ukpor clay percentages increased from 10 to 12%. Mould permeability was found to decrease from 11.00 to 7.00 by increasing the clay per cent from 10 to 22%. Ultimately, it was concluded that the Onitsha beach sand can be used for foundry applications.

Saikaew and Wiengwiset [10] determined the optimal proportion of bentonite and water to be added to the recycled moulding sand in order to reduce the defects in iron castings. The properties of the moulding sand investigated were of average compressive strength and permeability. The micro-structural analysis and Rockwell hardness test were performed on the iron cast parts. It was found that 93.3% of one-time reused moulding sand containing 1.7% water and 5% bentonite gave optimal sand mould properties, i.e. GCS of 53,090 N/m^2 and a permeability of 30 A.F.S. It can be seen from Table 1 that the average hardness of ferrous castings (5 nos) casted using optimized sand mixture is considerably more as compared to those made using usual sand mixture. It shows that the features of the castings are influenced by the sand mixture used for making moulds. During casting, the moulding sand's compressive strength regulated the capability to uphold its contour and exterior softness, while permeability regulated the capability of the moulding sand to permit removal of hot air and gases. The extent of permeability and surface smoothness of the moulding sand influences the discrepancy of uneven surfaces on the casting, leading to dissimilar hardness of the castings. The aforementioned condition arises in casting due to the variation in its microstructure, which will cause difficulty in machining of the cast material.

The microscopic images of two different types of castings are shown in Fig. 4. The cast iron surface possessed topographically coarse projections, which is considered as three-dimensional (3D) casting defect. These imperfections arose on the part surface at the time of pouring of the melt into the sand mould and resulted in spreading out of the sand. It can be seen that the casting obtained from the optimized sand mixture (Fig. 4b) was significantly smoother than that obtained from the conventional sand mixture (Fig. 4a), as

Table 1 Hardness value of castings [10]

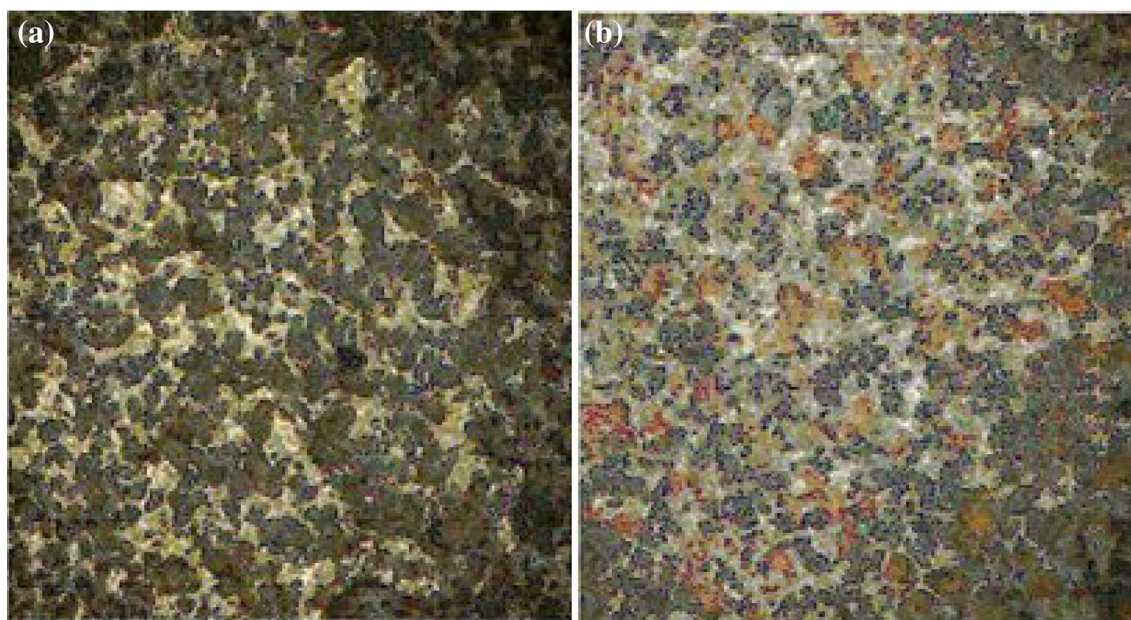| Sl. no.	Mould hardness when optimized sand mixture was used	Mould hardness when conventional sand mixture was used
1	18.90	17.80
2	18.30	16.63
3	18.53	16.57
4	17.57	17.00
5	18.70	17.57

Fig. 4 Micrographs of the castings obtained from **a** conventional sand mixture; **b** optimized sand mixture [10]

the distance between the peaks and valleys seems to be more in Fig. 4a. It was found that the quality of the optimized mixture-based sand mould was better with regard to that obtained from the usual one. However, the authors have not tested the strength of the iron castings obtained from both the sand mixtures. The comparison of mechanical strengths of the castings would have enriched their findings.

Chavan and Nanjundaswamy [11] used a variety of additives such as tamarind and coconut shell powders, and fly ash while preparing a sand mould from Olivine sand using clay as a binder. The average grain fineness number (GFN) of the moulding sand utilized for the experimental work was between 45 and 55. The sand mould consisting of coconut shell powder was found to exhibit higher compressive strength than that containing fly ash and tamarind powder at 1% of additive content. Similarly, tamarind powder containing mould showed higher collapsibility as compared to that of mould containing coconut shell and fly ash powders. During casting, the heat generated within the mould burns the excess additives and, subsequently, causes easy removal of the cast part. Permeability of the shells was almost the same, and this may be due to the coarse particle size of the additives. The properties of the moulding sand mixtures containing iron dust, coal dust and saw dust were investigated by Seidu and Kutelu [12]. It was determined that the GCS of 25% saw dust-modified mould was maximum, i.e. 108.99 kPa because it led to better mould compaction which is due to the superior moisture-attracting capacity of the saw dust than that of coal dust and iron dust-modified mould.
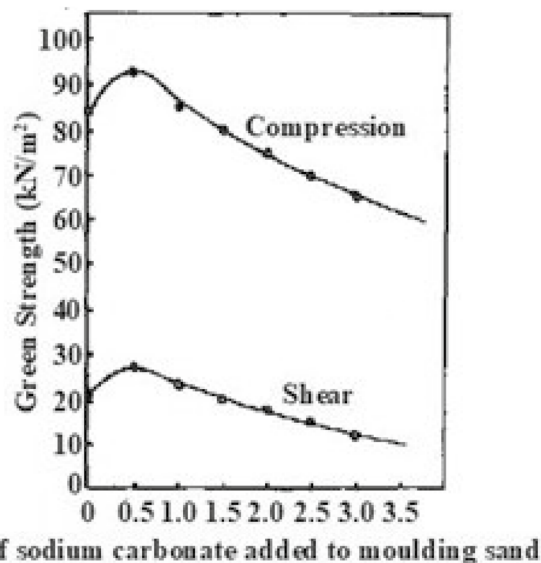

Fig. 5 Green strength versus % sodium carbonate for the moulding sand mixture [13]

Loto and Adebayo [13] analysed the moulding properties of sodium carbonate containing Igbokoda clay and silica sand. The influence of sodium carbonate in the sand mould on GCS and green shear strength (GSS) is shown in Fig. 5, and it is clear that the GCS and GSS are enhanced by the addition of sodium carbonate up to 0.5 wt%. However, further addition of sodium carbonate showed a decrease in GCS
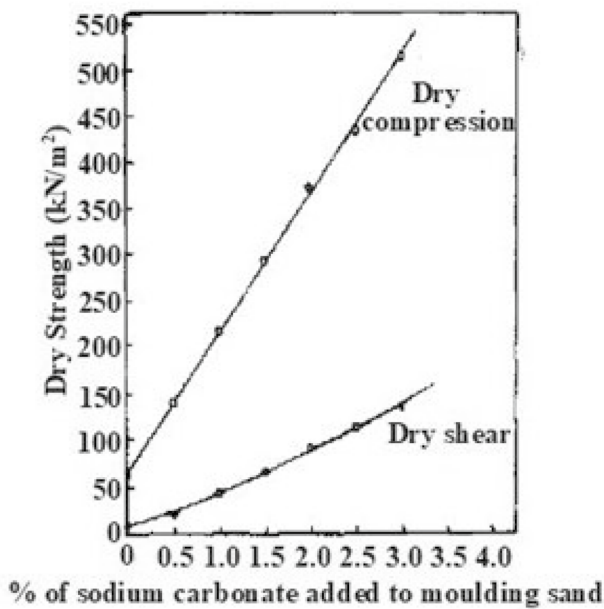
Fig. 6 Dry strength versus % sodium carbonate for the moulding sand mixture [13]
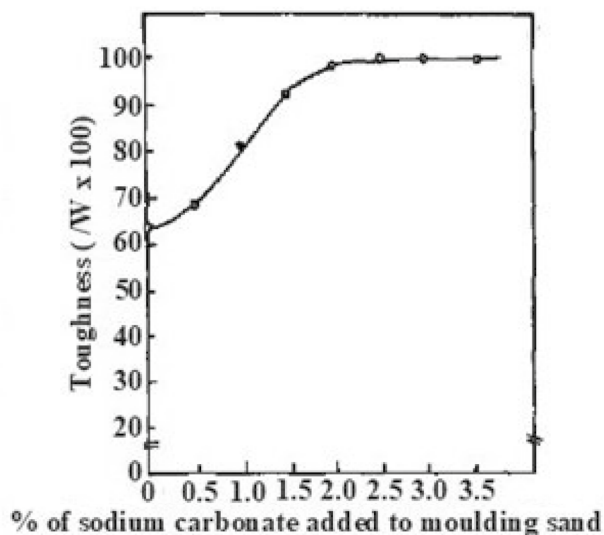

Fig. 7 Toughness versus % sodium carbonate for the moulding sand mixture [13]

and GSS. They also studied the effect of sodium carbonate addition in the moulding sand on DCS and dry shear strength (DSS) (Fig. 6) and toughness (Fig. 7). It is found that both DCS and DSS followed an increasing trend with an increase in the content of sodium carbonate. However, the toughness first increased gradually with a rise in sodium carbonate per cent up to 2 wt%; afterwards, it became approximately constant on further addition of sodium carbonate in the moulding sand mixture.
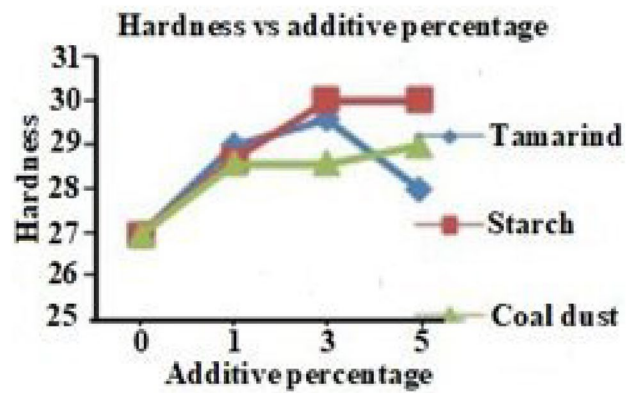

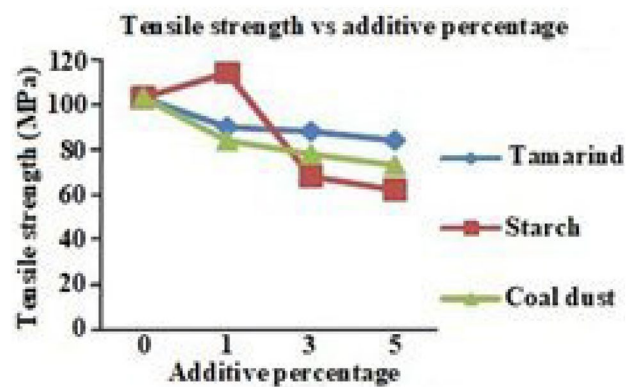**Fig. 8** Hardness versus additive percentage [15]

Fig. 9 Tensile strength versus additive percentage [15]

Rao and birru [14] investigated the effect of different percentages of molasses and fly ash additives on mechanical properties of green sand mould, and also the authors compared the mechanical properties of a modified green sand mould containing 2.25% molasses and 15% fly ash with that of the conventional sand mould without additives. It was ascertained that the modified green sand mould exhibited good compression strength of 185 kPa, the permeability of 260 and dry compression strength of 470 kPa. It was concluded that the modified green sand mould exhibited better moulding properties as compared to the unmodified (without any additive) green sand mould. Kumar et al. [15] examined the effect of starch powder, tamarind powder and coal dust at different proportions on mechanical properties, namely tensile strength and hardness of aluminium (Al) alloy casting. From Fig. 8, it is clear that the hardness of Al alloy casting obtained from sand mould containing starch powder is the highest as compared to that obtained from other additives. They found that tamarind powder and coal dust in sand mould gave better compressive strength; however, there was a drop in tensile strength of the Al alloy casting obtained

from the sand moulds containing the aforementioned additives due to decrease in mould permeability owing to their fine grain size (Fig. 9).

Okonji et al. [16] investigated the suitability of ant hill powder and groundnut shell ash as binders for producing sand moulds and cores in the foundry industries in Nigeria. The mould properties tested were particle size, green strength, moisture content, mouldability and permeability. It was found that the sand moulds containing 30% ant hill powder and 14% groundnut shell ash exhibited the aforementioned properties within the accepted limits for both non-ferrous and ferrous castings. As per Khandelwal and Ravi [17], chemically bonded sand moulds exhibit better mould properties and the castings produced using these moulds are found to have a high rate of dimensionally accuracy. They investigated the influence of aforementioned sand's grain size, binder content plus curing time on mould properties, namely compression strength, shear strength, core hardness and mould as well as core shrinkage. It was found that the mechanical properties augmented with rise in binder content and reduced with increase in grain fineness number. Although all the parameters were significant in influencing the mechanical properties of the sand mould, the curing time was found to be the most significant among them. It was found that the core shrinkage augmented with augmentation in all the chosen parameters; however, sand grain size was the most significant parameter influencing the core shrinkage. In case of chemically bonded sand mould, these phenomena occur due to their bonding characteristics and curing mechanism. When the silica sand is mixed with a chemical binder, a very thin layer of binder is formed on individual sand grain which when combining with another sand grain forms a resin bridge. Curing mechanism is used to shorten these resin bridges owing to solvent evaporation which is present in the binder, thereby causing hardening of the bridges. They conducted SEM analysis of the chemically bonded sand grains to view the bonding mechanism clearly as shown in Fig. 10.

Orumwense [18] carried out a comparative study on the moulding properties of synthetic sand mixtures containing locally available sand and different percentages of Enugu fireclay and Upkor clay possessing a variable degree of plasticity. Upkor clay was found to be a better sand binder than Enugu fireclay. Moreover, he obtained the optimum sand mould properties at sand mixtures containing 8 wt% fireclay, 10 wt% Ukpor clay and 3 wt% water. It was found that the aforementioned synthetic sand mixture can be used for general purpose casting as well as steel casting. Lidumnieks et al. [19] studied the effect of mould sand compositions containing variable per cent of bentonite, water and coal dust on cooling capacity or heat absorption of the green sand through Fourier thermal analysis. It was
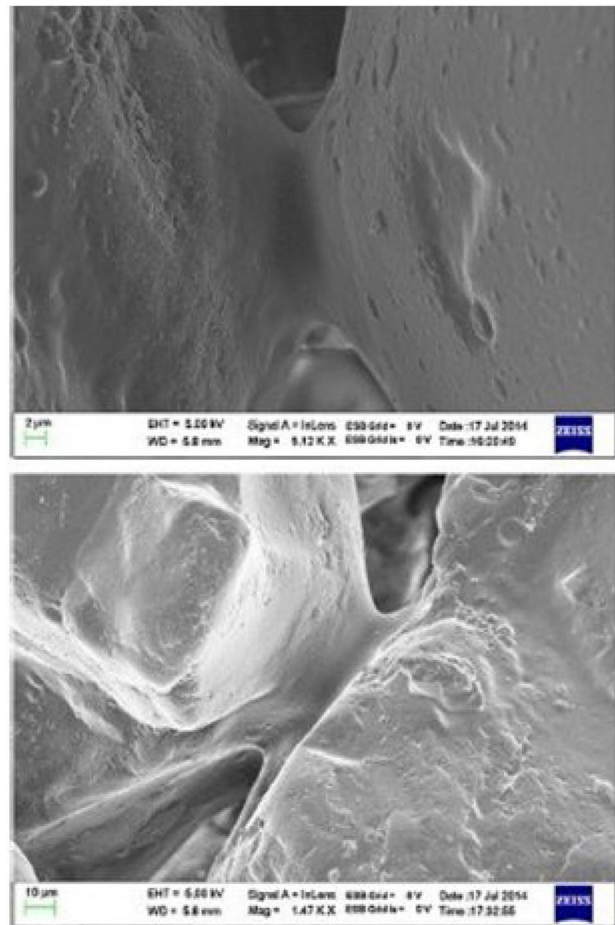

Fig. 10 SEM micrograph shows irregular sand grains bonded with alkyd resin [17]

found that the green sand mould composition drastically affected the cooling capacity and heat absorption rate of the sand moulds. Increase in bentonite and water content was found to increase the chilling capacity of the sand mould and it was maximum between 400 and 1000 °C. Addition of coal dust enhanced the heat absorption rate of the sand mould at 150 °C and between 250 and 600 °C. It is assumed that the cooling rate affects the solidification rate, which governs the final microstructure of the casting.

From the critical analysis of the above studies, it is concluded that the locally available sands and clays can be used as moulding material for producing moulds for sand casting. Similarly, various additives that can be added to improve significant mould properties are sawdust, coal dust, ant hill ash, tamarind powder, fly ash, coconut shell powder, molasses, groundnut shell ash, etc. However, it is essential that the important shell properties such as GCS, GSS, DCS, DSS, permeability and shatter index need to be determined prior to their usage as casting moulds.
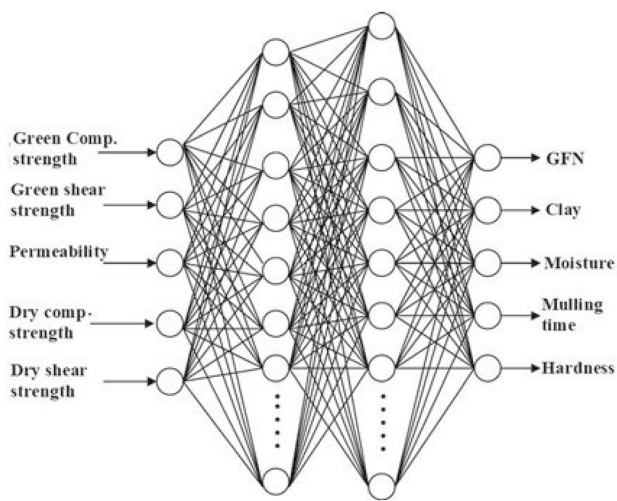
Fig. 11 Backward modelling network [21]

2.2 Modelling of Sand Mould Properties

The composition of the moulding sand is one of the sources of defects in sand casting. These imperfections can be reduced significantly by appropriate control of sand mould properties, which depends on many input variables. Therefore, it is essential to determine the relationship between the mould properties and various input variables. Parappagoudar et al. [20] used DOE along with response surface methodology (RSM) to generate models in order to analyse the relationships existing between the inputs and outputs of the foundry sand mould system. The input variables selected were GFN, clay%, water% and degree of ramming and GFN, permeability, mould hardness and bulk density as outputs. A linear model was developed using full-factorial DOE, whereas nonlinear model was developed using the central composite design (CCD) and Box–Behnken design. A statistically adequate model providing minimum error % was judged as the best model. The models were validated using 20 random test cases. It was found that CCD exhibited the best performance in forecasting GCS and permeability, whereas DOE showed good attainment in predicting mould

hardness and bulk density. The above work by the authors would help a foundry man to build a proper model for predicting different sand mould properties correctly.

Artificial intelligence methods appear to be a potentially valuable way to control the properties of different sand mixtures. Karunakar and Datta [21] built up an artificial neural network (ANN) model with input parameters, namely GSS, GCS, DCS, DSS and permeability. The responses of the ANN model were clay percentage, grain fineness number, moisture percentage, hardness and mulled time. Further, they also used a genetic algorithm (GA) to control the green sand mould properties. On the basis of the aforementioned inputs and outputs containing experimental data, a back propagation neural network (BPNN) model was made and trained for the purpose of efficient forecasting (Fig. 11). ANN and GA programmes were run using MATLAB software, and the results obtained by these tools were compared, as shown in Table 2. The set of best possible parameters which yielded the set of needed mould properties was searched by ANN and GA techniques. It was found that the percentage errors predicted by ANN were considerably high in a few cases as compared to GA. The percentage error produced by GA was found to be more than that of as generated by ANN only in the prediction of GFN, which was perhaps due to the choice of optimal properties. The more inaccuracy of results predicted by ANN was due to the fact that ANN produces results subsequent to the normalization of the data and, then, denormalizes the forecasted value. However, GA produces results via coding along with decoding of the factor settings.

Further, Babu et al. [22] developed both an adaptive neuro-fuzzy inference system (ANFIS)/neuro-fuzzy and BPNN models to forecast the GCS of moulding sand mixtures. The composition of the moulding sand is mentioned in Table 3. Fuzzy neural network develops a rule viewer to forecast the response using the trained fuzzy inference system. Both input process parameters and output parameter were same for neuro-fuzzy and BPNN models. From Table 3, it is clear that the maximum error percentages between the actual and predicted results by BPNN and neuro-fuzzy models are 20% and 9.9%. Authors clearly observed that the moulding sand properties were predicted

Table 2 Error percentage in the forecast of results by ANN & GA [21]

Sl. no.	Input parameter	Experimental result	Results predicted by ANN	Results predicted by GA	% Error produced by ANN	% Error produced by GA
1	GFN	38.03	37.41	39.88	1.63	−4.87
2	Clay per cent	4	5.08	4.75	−27.0	−18.75
3	Moisture per cent	5	6.05	5.93	−21.0	−18.6
4	Mulling time (min)	5	5.21	5.32	−4.2	−6.4
5	Hardness (N/m^2)	390,040	449,820	403,760	−15.32	−3.51

Table 3 Error % in the forecast of results of the moulding sand mixture by ANFIS and BPNN [22]

Sl. no.	Coal dust (%)	Clay (%)	Moisture (%)	Mulling time (min)	GCS (g/cm^2)				
					Actual value	Predicted value by BPNN	% Error	Predicted value by neuro-fuzzy	% Error
1	0	4	5	6	612	586.66	4.14	551	9.96
2	2	4	4	4	774	758.23	2.037	740	4.39
3	2	4	6	6	630	648.58	2.95	575	8.7
4	4	4	6	8	747	730.98	2.14	673	9.9
5	6	4	5	6	774	815.03	5.3	810	4.65
6	0	6	4	4	897	958.77	6.88	966	7.69
7	0	6	6	8	793	664.11	16.25	733	7.56
8	2	6	4	6	1065	1227.9	15.3	1050	1.4
8	4	6	3	8	1130	1119	0.95	1130	0
10	6	6	3	6	950	857.69	9.71	960	1.05
11	6	6	6	4	974	986.4	1.27	917	5.84
12	0	8	5	6	995	953.94	4.12	1070	7.5
13	2	8	4	8	1257	1267.3	0.82	1270	1.03
14	4	8	3	6	800	641.13	19.85	871	8.875
15	4	8	6	4	1145	959.78	16.17	1070	6.5
16	6	8	4	8	1335	1427.1	6.89	1330	0.0375

Table 4 Percentage contribution and optimum parameter levels on casting defects [24]

Symbol	Parameter	Mean casting defect (%)	S/N ratio of casting defects (%)	Optimum levels	Optimum value
A	Moisture content (%)	6.9	7.66	2	2.6
B	Green strength (g/cm^2)	72.2	71.16	3	950
C	Permeability (number)	–	–	1	235
D	Mould hardness (no.)	13.43	13.90	2	80

more precisely by the neuro-fuzzy model than the BPNN model, due to its capability of high learning accuracy and generalisation. Furthermore, the neuro-fuzzy model necessitates little learning time with regard to BPNN.

Singha and Sing [23] developed an ANN model with input parameters, namely moisture content, permeability, pouring temperature, GCS and number of vent holes in the sand mould. The outputs of the ANN model were expansion defect, gas defect and weak sand defect. MATLAB software was used to run the ANN program containing three layers, i.e. input layer, output layer and a hidden layer. They found that the optimized results of the defects were expansion defect of 6.23%, gas defect of 7.28% and weak sand defect of 5.74%. These results were found to be similar to the previous results obtained by Taguchi method. The authors beautifully explained the usability of ANN model in predicting the aforesaid defects, but they did not determine the mechanical properties of the casting obtained from the prepared sand mould.

Guharaja et al. [24] examined the effect of process parameters (green strength, moisture content, permeability and mould hardness) on the defects caused while casting spheroidal graphite cast iron. They used Taguchi's method to find out the most favourable parametric settings. Further, analysis of variance (ANOVA) and signal-to-noise (S/N) ratios were used for predicting the casting defects. Table 4 shows that the parameters, namely moisture content, mould hardness and green strength, influenced both mean and S/N ratio of the casting defects, whereas the parameter permeability did not affect them. They found that the casting defects were 25% before application of Taguchi's method, and after that, it was reduced to 3.25% on the whole. However, they did not consider the sand particle size, pouring temperature and pouring time of the molten metal while casting.

Upadhye and Keswani [25] optimized the process parameters using Taguchi method in sand casting and found that the casting defects was reduced to 37.66% by maximizing the S/N ratios and diminishing the noise factors. The parameters considered were green compression strength, moisture content, pouring temperature, sand's particle size, permeability, pouring time, mould hardness and pressure test. They found that S/N ratio increased from -15.544 to -9.689,

Table 5 Per cent contribution and optimum parameters under economic consideration [26]

Control parameter	Mean casting defect (%)	S/N ratio of casting defects (%)	Optimum value	Optimum level
Moisture (%)	11.41	16.58	4	1
Green strength (g/cm^2)	8.32	13.77	1990	3
Pouring temperature (°C)	6.12	8.87	1410	3
Mould hardness (V) (No)	5.22	10.23	72	1
Mould hardness (H) (No)	4.22	7.78	85	2

which indicated the reduction in casting defect. Kumar et al. [26] also used Taguchi's optimization technique to control the input process parameters, i.e. green strength, moisture content, pouring temperature and mould hardness to reduce casting defects of grey cast iron (GCI). It is clear from Table 5 that the mean and variance of the casting defects are affected by all the process parameters. They determined the best possible value of each selected process parameter in order to decrease the casting defects. It was found that there was a rise in product yield after the application of Taguchi's method, due to a decrease in casting defects from 5.185 to 3.363%.

In a green sand mould, the worth of castings is affected by its characteristics, namely GCS, GSS, permeability, etc., which depends on control/input parameters. The relationship of the aforementioned characteristics/responses with the chosen input parameters such as sand grain's size and shape, and binder is actually very complicated. Previously, the assessment of green sand mould properties was carried out on the basis of usage of different additives and it has been found that these additives act as boosters to augment definite sand mould properties. Surekha et al. [27] did multi-objective optimization of green sand mould properties, particularly GCS, hardness, permeability and bulk density using both GA and particle swarm optimization (PSO). The control (process) factors were GFN, water%, clay% and number of strokes. They developed nonlinear regression equations amid the selected input and output parameters to predict the responses beforehand using aforementioned methods. It was found that the % error between the predicted and the experimental results was less by the PSO method than that by the GA method.

From the above analysis, it is seen that modelling and optimization methods such as regression analysis, RSM, ANN, Taguchi method, PSO and GA can be very well used to predict and optimize the significant moulding sand properties, which are essential for producing qualitative castings.

2.3 Rapid Manufacturing of Sand Mould

Rapid manufacturing (RM) is defined as application of computer-aided design (CAD) base additive manufacturing process to build the components which are directly used as finished parts [28–30]. RM is especially useful for manufacturing very complicated and delicate parts which would have been either impossible or difficult to manufacture by conventional sand moulding process [31, 32]. In this method of 3D printing technology, first the CAD file of the final component is translated into stereolithography (STL) file, and later, it is converted into Common Layer Interface (CLI) file that have geometric information of each layer. Eventually, the component is made layer by layer until its completion. Sand mould 3D printing is of two types, out of which one is based on selective laser sintering (SLS) process, while the other method uses the principle of micro-droplet to construct sand moulds [33, 34].

In SLS process, the laser is used to bind the sand particles. On the other hand, sand mould 3D printing technology supported by the micro-droplet jetting principle (MJP) utilizes a droplet nozzle to spray the adhesives on the surface of the sand particles which are intermixed with the curing agent. The adhesives react with the curing agent for proper bonding [35]. The commonly used adhesives are a phenolic resin, furan resin and inorganic adhesives based on silicate and phosphate. The properties of the sand mould are influenced by the cross-linking reaction rates between the curing agent and the adhesive. Too fast or too slow reaction rates are not desirable as they adversely affect the quality of the sand moulds. Usually, different cross-linking reaction rates are obtained for different per cents of curing agent, owing to their different viscosities [36]. Guo et al. [37] studied the influence of viscosity and curing agent on the flowability of damp silica sand grains. These grains were mixed with two curing agents of variable viscosities, and Jenike shear test was employed to determine the flow characteristics of moist sand grains, viz. effective internal and wall friction angles, major consolidation stress and unconfined yield strength. It was found that an increase in the per cent of curing agent led to increase in cohesion and decrease in effectual internal friction angle amid the silica sand grains, but it adversely affected the flowability of the sand grains.

Hawaldar and Zhang [38] manufactured cast iron (FG260) pump bowls using both conventional no-bake sand casting mould and 3D-printed MJP mould, as shown in Fig. 12.
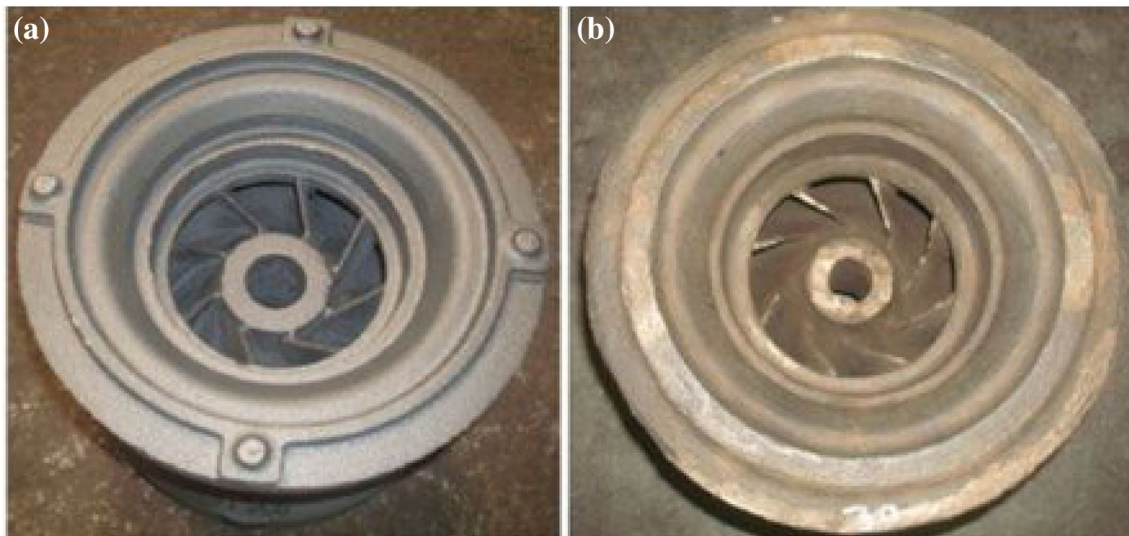
Fig. 12 CI pump bowl made by using **a** 3D printed mould; **b** conventional sand mould [38]

Table 6 Specifications of the pump bowl

S. No.	Name of the component	Dimension (mm)
1	Overall size (dia × height)	247 × 220
2	Thickness of the wall	7
3	Thickness of the vane	4
4	No. of vanes	8

The dimensions of the pump bowl are given in Table 6. The authors compared the efficiency of both processes in terms of sand used, design allowances, metal used and fettling work. The 3D printing process was found to be more effectual as compared to the conventional sand casting process when the requirement of moulds is less due to less consumption of sand, metal, reduced fettling work and design allowances. Further, the surface finish of 3D printed mould was found to be better than that obtained by the conventional process, which is due to the fact that 3D-printed sand moulds along with the core possess close tolerance. In 3D printing, the main goal is to achieve the dimensional accuracy of the parts rather than achieving other sand mould characteristics, viz. strength, permeability and density due to difficulty in controlling these mould properties consistently over the entire volume of the printed parts [39–41]. However, sand mould should possess sufficient mould permeability for proper melt filling and possess sufficient strength for easier handling. The binder should have low volatile content in order to avoid porosity defects in casting.

Coniglio et al. [42] investigated the effect of print resolution, sand conveyor/recoater speed (RS) plus job box position on permeability and strength of the sand moulds. The binder used for printing sand moulds was furan, and the
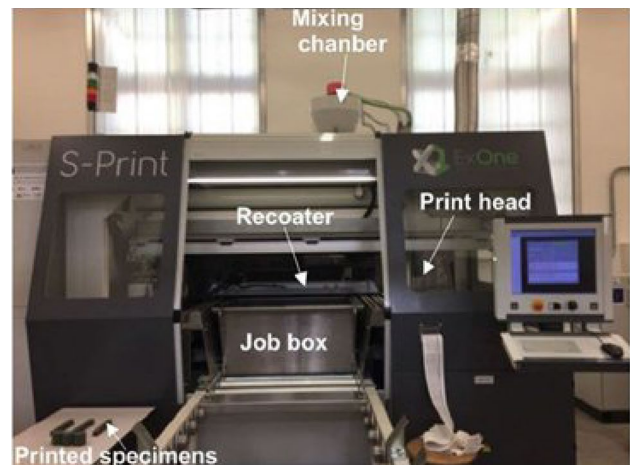

Fig. 13 Overview of 3D sand mould printer [42]

jetting printer was furnished with a job box of dimensions $800 \times 500 \times 400$ mm^3, as shown in Fig. 13. Eight kilograms of sand was mixed with the catalyst sulphonic acid and inhibitor magnesium. Each sand layer of 280 μm thickness was sequentially settled on the job box. The process was carried on till the last layer of the sand specimen was printed. Then, the printed sand samples were cured at room temperature for an hour within the job box and the lose sand grains were taken away via a soft brush or else compressed air. It was found that the mould properties depended on the process parameters, RS and print resolution and their positions inside the job box in the course of the printing process. RS controlled both permeability and strength, whereas the print resolution merely influenced the sand mould strength. Slow RSs are to be used if small sand mould permeability
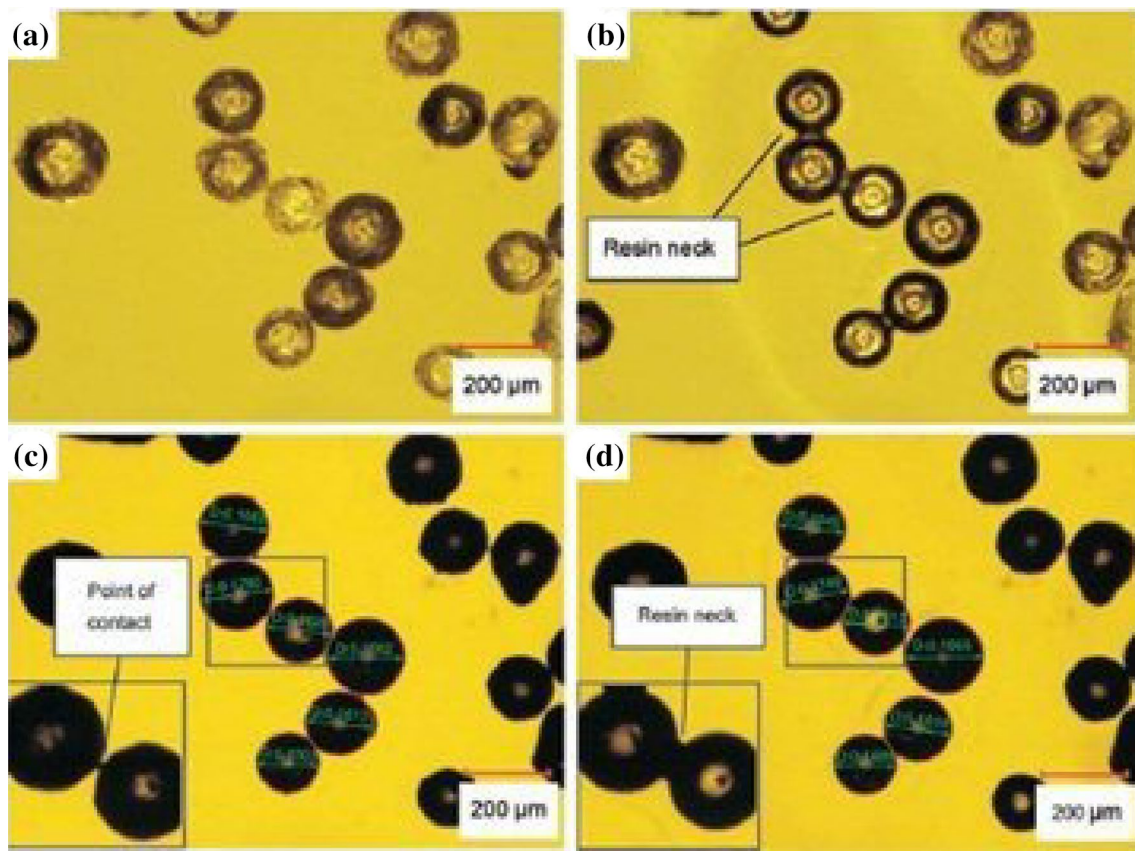
Fig. 14 Microscopic images of coated ceramsite sand **a** before laser heating, **b** after laser heating with upper-light and back-light on, **c** measurement of diameter before laser heating with upper-light off and back-light on, **d** measurement of diameter after laser heating with upper-light off and back-light on [44]

is required. On the other hand, sand moulds produced using fast RSs to achieve higher mould permeability cause aniso-tropic properties of the sand samples inside a given job box.

3D sand moulds undergo a post-curing process to achieve the ultimate strength [43]. The resin covered on the surface of the sand particle shifts to the contact points of the neighbouring particles at some stage in the post-curing process. Thus, the vanishing of the resin film on the particle surface results in a reduction in the space sandwiched between the particles, which produces macroscopic contraction and distortion of the parts. Zhao et al. [44] explored the effect of resin flow on shrinkage characteristics of ceramsite-coated 3D sand moulds. Ceramsite, one kind of artificial sand, possesses higher refractoriness as compared to quartz sand. This sand requires less resin per cent to obtain the identical strength of coated quartz sand owing to its more spherical structure (Fig. 14), which decreases the production of gas and increases the mould permeability to attain better quality castings.

The authors measured the diameters of coated ceramsite in order to determine the relationship amid the particle diameter and resin coating thickness. It was established that for resin content of 2 wt%, the resin coating thickness enhanced from 0.8 to 2.3 μm when the particle diameter increased from 107 to 500 μm. The shrinkage ratio was found to first decrease, and then, it amplified as the particle diameter enhanced. The experimental result of minimum shrinkage ratio was found to be 3.28%, and the resultant particle diameter was found to be 300–375 μm. Mitra et al. [45] investigated the effects of curing temperature and time on permeability and three-point bend test on 3D-printed sand moulds containing furan binder. It was found that the permeability of the sand specimen reduced with a rise in temperature owing to the shrinkage of the sand mould. When the sand samples were cured at 100 °C, there was not any considerable change in the mechanical strength of the printed sand specimen. It was found that the stored printed moulds can be used for casting, and their permeability and strength values remained the same. Sivarupan and Mansori [46] identified the effect of RS, one of the 3D sand mould printing parameters, on the pore structure and permeability for improved casting yield. It was found that at critical recoater speed, i.e. 0.182 m/s, the permeability values seem to diminish the disparity along the job box coordinates. At RS of 0.286 m/s, intrinsic cracks
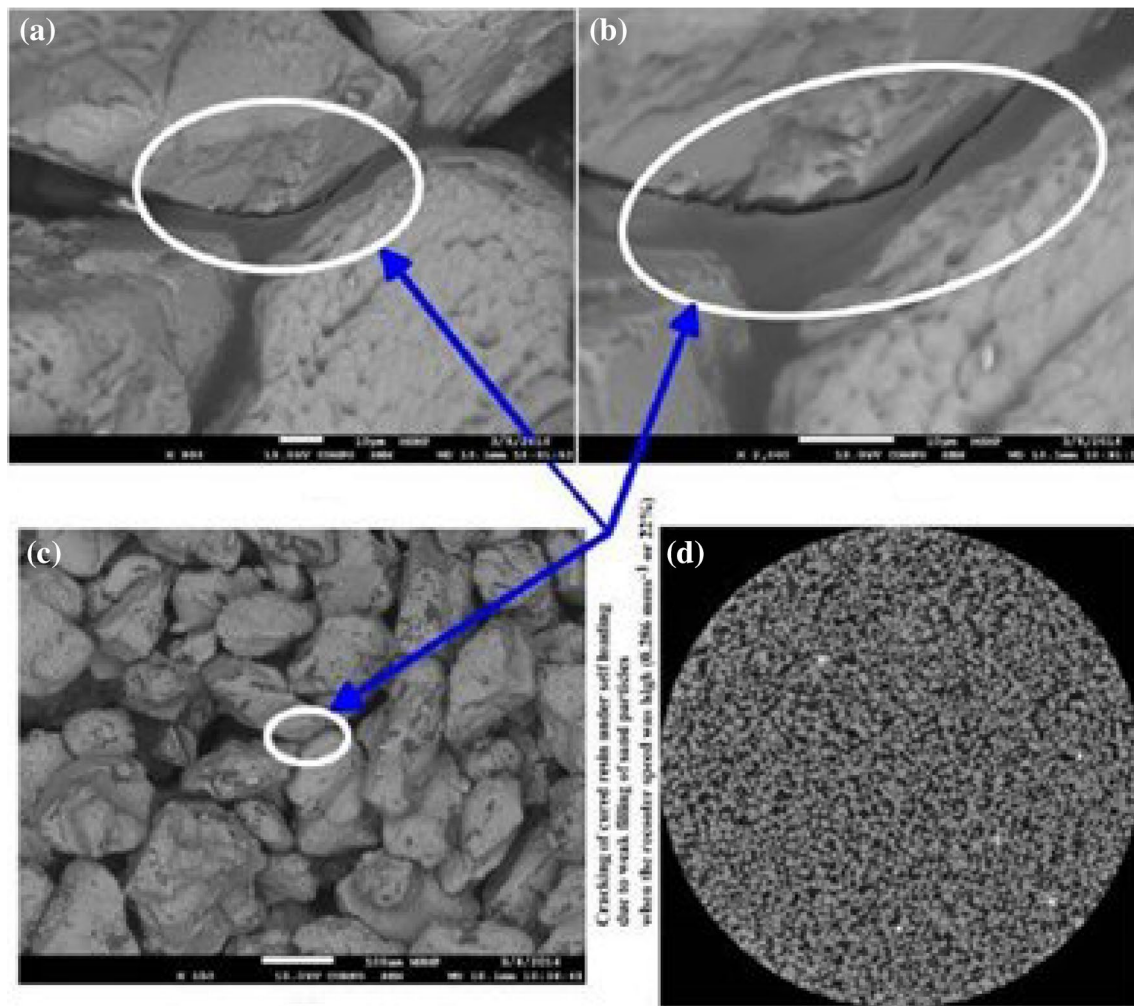
Fig. 15 Backscattered electron images showing cracks of cured resin under self-loading due to weak filling of sand particles at high RS, i.e. 0.286 m/s [46]

on the furan bridges linking the sand grains were found as shown in Fig. 15.

From the above study on 3D printing of sand moulds, the various process parameters are found to be curing temperature, curing time, recoater speed, print resolution, etc. The various adhesives and sands used for printing sand moulds are furan, phenol, inorganic resins, etc. and silica, chromite, etc., respectively. The main objective is achieving dimensional accuracy of the parts. It has been found that controlling other mould properties such as strength and permeability is quite difficult. The process has both advantages and disadvantages. It eliminates the usage of time-consuming pattern making a step of sand casting. Any complicated shaped mould can be effortlessly made by this process. It helps in prototyping a new design of a product. Limitations of the process include high initial and maintenance costs, high material cost, limited production volumes, etc., due to which it cannot be used by small foundries. It is

essential that the cost of materials for 3DP of sand moulds to be reduced so that the process can be accepted by all. Printing of sand moulds is comparatively much slower than conventional sand mould building process. However, until now, very limited studies have been done on establishing the relationships between printed mould properties and processing parameters. Thus, this area requires more intensive research to commercialize the process.

3 Effect of Processing Conditions on the Mechanical Properties of As-Cast/ Heat-Treated Materials

3.1 Ferrous Materials

Cast irons, constituting of ferrous alloys, have an extensive variety of mechanical properties. They can be casted into any

Table 7 Influence of boron as modifier on the mechanical properties of GCI [48]

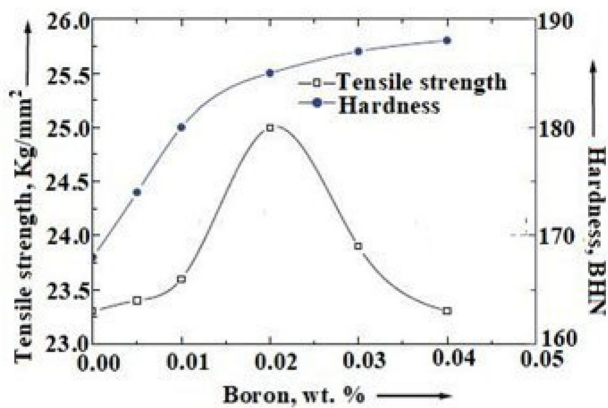| Sl. no.	Boron weight (%)	Tensile strength (kg/mm^2)	Hardness (BHN)
1.	0.000	23.3	168
2.	0.005	23.4	174
3.	0.01	23.6	180
4.	0.02	25.0	185
5.	0.03	23.9	187
6.	0.04	23.3	188

Fig. 16 Influence of boron wt% on casting's tensile strength and hardness [48]

shape and are mostly appropriate for manufacturing engineering components. Although, ferrous casting has superior properties such as outstanding castability, good mechanical and physical properties, grey cast iron (GCI) offers a unique versatility at a lower cost which could be obtained through microstructure control. The mechanical properties of GCI rely on its microstructures which are formed on solidification. In GCI, the elements usually added in trace amounts are boron (B), bismuth (Bi), lead (Pb), titanium (Ti), etc., and these elements significantly affect the properties and graphitic structure of GCI [47].

Ankamma [48] investigated the effect of boron addition at different proportions (up to 0.04%) on properties, namely tensile strength and hardness of grey cast iron. The value of Young's modulus of elasticity (E) in most of the technical handbooks was mentioned in different units, but now it has been standardized in SI units as N/m^2 or N/mm^2 to avoid very large numbers. As the author has determined the tensile strength of GCI using different additives in kg/mm^2, the present manuscript involves the same unit without converting to SI unit to show their original results by means of tables and graphs. Brinell hardness test was performed by the usage of a standard hardness testing machine. From Table 7 and Fig. 16, it is clear that with an increase in the amount of boron up to 0.02%, the tensile strength along with hardness values of the casting increased from 23.3 to 25.0 kg/mm^2 and 168 to 185 BHN. This is due to the formation of boron carbide. While the addition of boron beyond 0.02 wt% reduced the casting's tensile strength owing to the creation
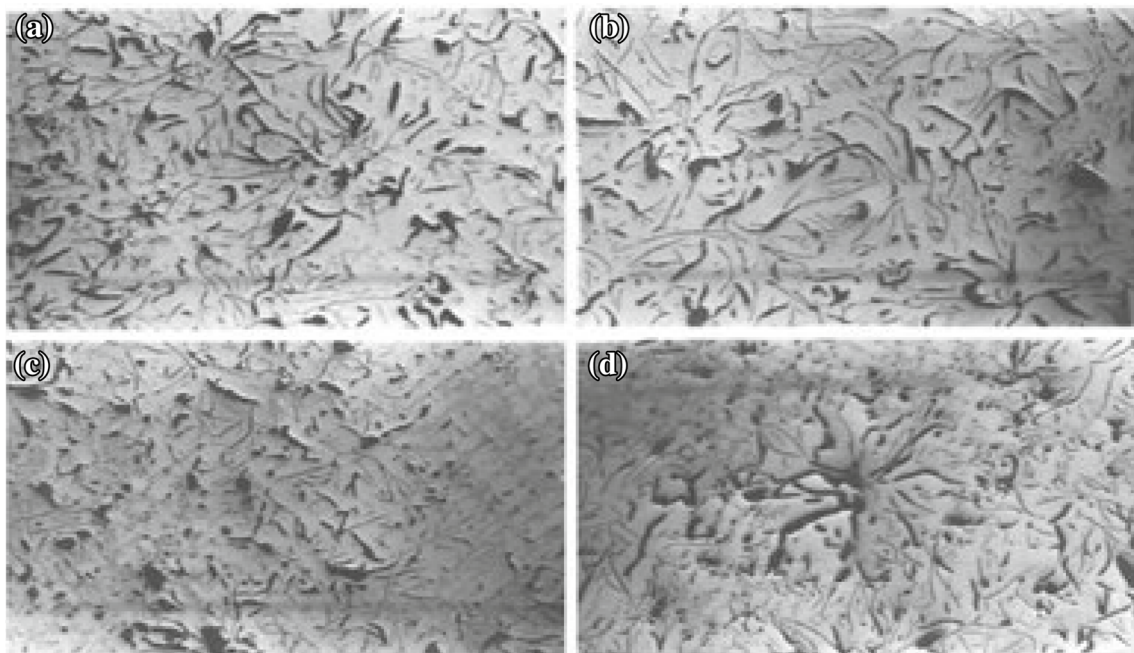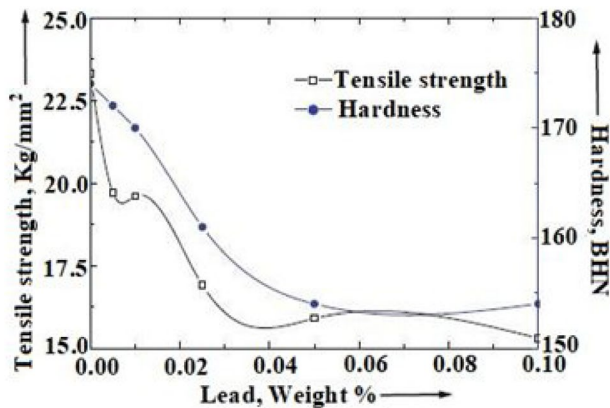

Fig. 17 Influence of boron wt% on the microstructure of GCI at ×100 magnification, **a** base iron with 0.00% B, **b** 0.02% B, **c** 0.03% B, **d** 0.04% B

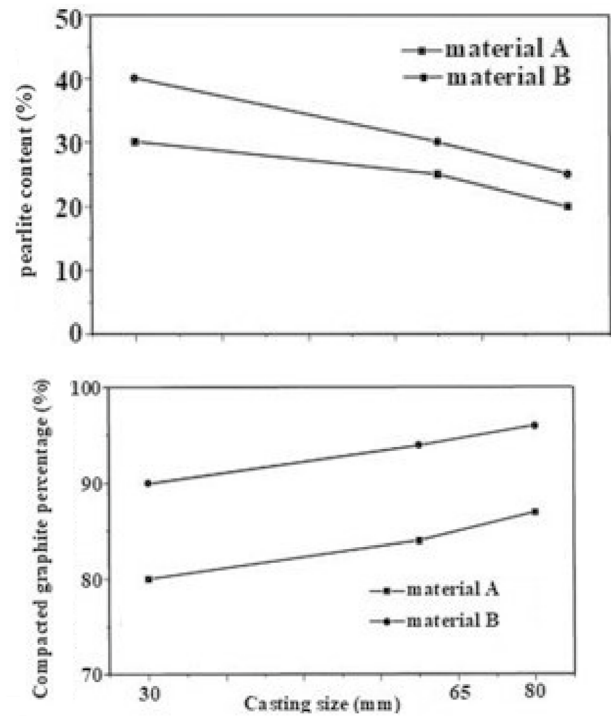**Table 8** Influence of lead wt% on casting's tensile strength and hardness [48]

Sl. no.	Lead weight (%)	Tensile strength (kg/mm^2)	Hardness (BHN)
1	0.000	23.3	174
2	0.005	19.7	172
3	0.01	19.6	170
4	0.025	16.9	161
5	0.05	15.9	154
6	0.10	15.3	154

Fig. 18 Influence of boron wt% on casting's tensile strength and hardness [48]

Fig. 19 Casting size versus different percentages of pearlite content and CG for materials A and B [49]

of types B and D graphites (Fig. 17), a mild rising pattern is seen with the hardness values.

Ankamma [48] also investigated the effect of lead addition at different wt% on properties of GCI. It is observed that with the rise in the amount of lead percentage, the tensile strength along with the hardness value of the casting diminished. Table 8 and Fig. 18 show that the tensile strength diminished from 23.3 to 15.3 kg/mm^2, whereas casting hardness diminished from 174 to 154 BHN. The quantity of pearlite too reduced on adding lead due to the development of thorny or meshes-type graphite in the microstructure.

Shy et al. [49] examined the different mechanical properties of cast iron without and with trace element addition of Ti, and the materials were named as material A (without Ti) and material B (with Ti addition). Figure 19 shows that the proportion of compacted graphite (CG) amplified with the addition of Ti, whereas the quantity of pearlite reduced when there was a rise in casting size and decrease in its cooling rate. Material B exhibited increased CG percentage for comparable casting size owing to the anti-spheroidizing impact of Ti. Figure 20 shows that the hardness decreased a bit with increase in section size for both materials A and B. Impact value decreased with the

increase in casting size because of the presence of additional interconnected graphites which aided easier generation of cracks so as to fracture the impact specimens. The impact value for material B was found to be lower than that of material A because of increased CG%. The authors observed that increase in section size did not change the mechanical properties of the casting significantly, even though the impact value reduced and a very small decrease in hardness was also observed.

Collini et al. [50] investigated that in GCI, the graphite content in the matrix directly influences both elongation to failure as well as elastic modulus. Figure 21 shows that with an increase in graphite percentage, both the elongation to failure and elastic modulus values decrease. Figure 22a shows that with the increase in graphite content, the mean threshold stress intensity factor (SIF) decreases, and Fig. 22b shows that a low average lamella length produces utmost fatigue resistance of GCI. Furthermore, the authors found that the change in tensile strength and decline in elastic stiffness occurred owing to the initiation of micro-crack under loading at the lamella tips. The range of threshold stress intensity factor of the actual materials is influenced by the quantity of graphite inserted into the matrix. The authors clearly observed that the graphite lamella's mean length showed a superior co-relation with the fatigue limit of the material, and also the mechanical properties varied with the graphite content. Figure 22 shows that both fatigue limit
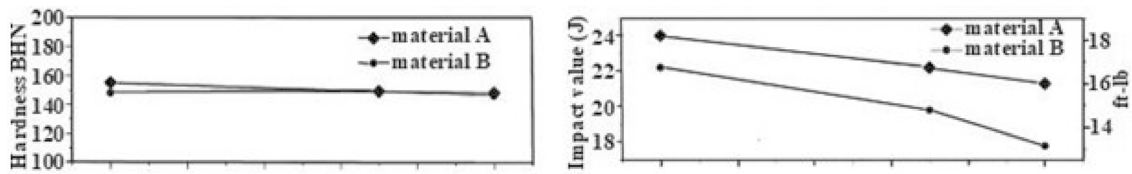
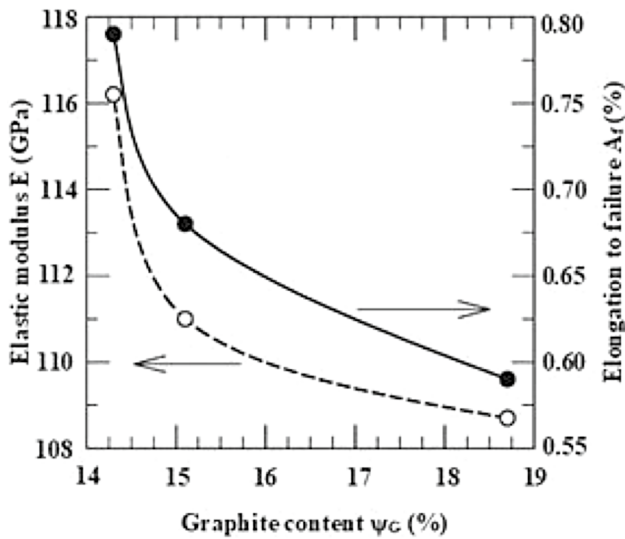**Fig. 20** Casting size versus hardness and impact value of materials A and B [49]

Fig. 21 Influence of graphite percentage on elastic modulus and elongation to failure of GCI [50]

and threshold SIF decease linearly with increasing graphite content in cast iron.

The cooling rates greatly influence the microstructure as well as mechanical properties of GCI. The high cooling rate produces a fine structure which causes an increase in strength of cast iron. It also affects both dendrite arm spacing (DAS) and secondary dendrite arm spacing (SDAS). Behnam et al. [51] observed that both DAS and SDAS lessen with the rise in cooling rates. Fine dendrites are produced by fast cooling rates, while big and coarse dendrites are created by slow cooling condition. The hardness value increases with the increase in cooling rate because the higher cooling rate produces fine dendrites. Authors found that the hardness is reduced because the cooling rate decreases, but they did not examine the effect of cooling rate on tensile strength and fatigue strength of GCI.

High chromium cast irons (HCCIs) are mostly used in milling, mining and manufacturing industries which need materials possessing extraordinary abrasion and corrosion resistance properties. HCCIs mostly contain rigid M_7C_3-type carbides. Hypereutectic HCCIs possess additional volume fractions of the M_7C_3 carbides in relation to hypoeutectic HCCIs. Inoculants are substituted in the alloy at the latter stage to augment the number of nucleation sites for faster solidification to increase the casting quality [52]. Adding up of several inoculants, for example, magnesium, boron, titanium, etc. to the matrix/carbide interphase, leads to modification of the eutectic carbide structure. Qu et al. [53] investigated about the influence of cerium (Ce) on the as-cast microstructure of a hypereutectic HCCI. It is quite apparent from Fig. 23 that the carbides are modified steadily and the morphology of M_7C_3-type carbides turned into more isotropic, when there is an augmentation of Ce in the alloy; however, the conversion was slightly sluggish when Ce addition exceeded 1.0 wt%. The authors observed that the addition of cerium to the matrix/carbide interphase developed the size and morphology of the eutectic carbides.

Fig. 22 Influence of **a** graphite percentage on threshold SIF; **b** mean length of lamellas on fatigue limit of GCI [50]
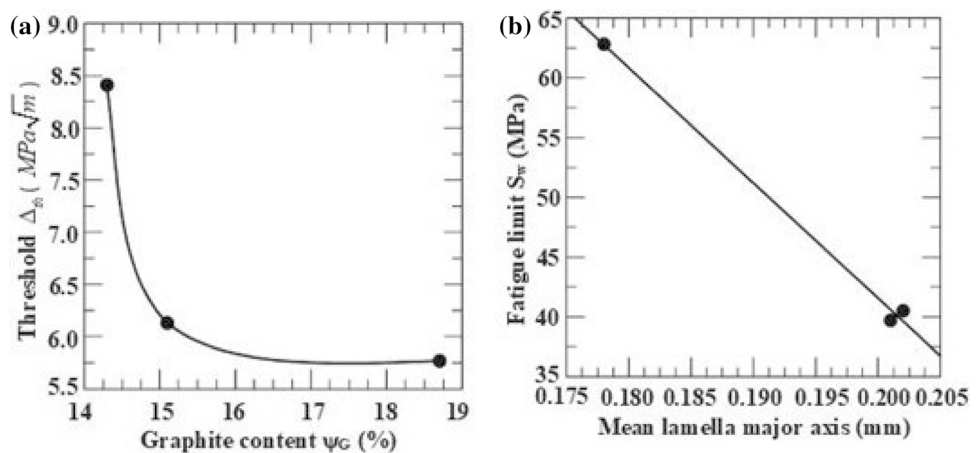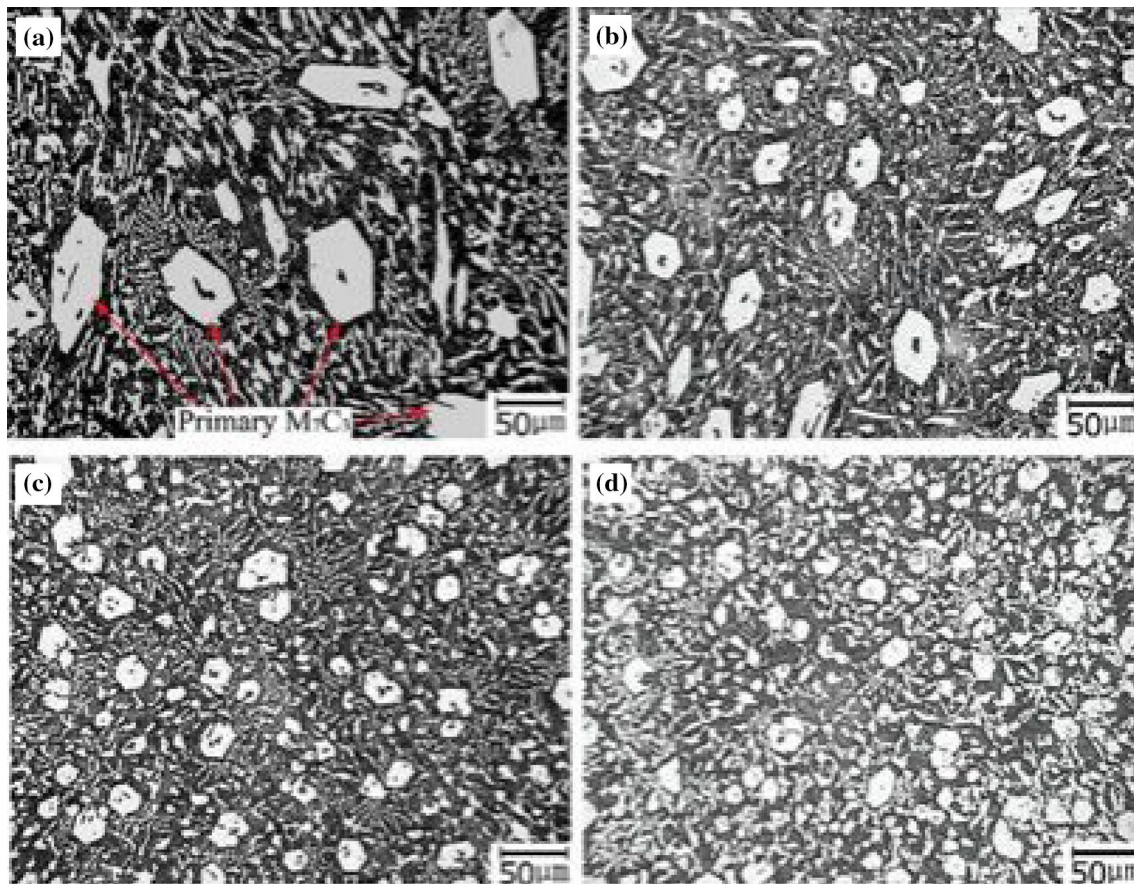
Fig. 23 Microstructures of hypereutectic HCCI containing different wt% of Ce. **a** 0.0 wt%, **b** 0.5 wt%, **c** 1.0 wt% Ce, **d** 1.5 wt% Ce [53]

Ruiz et al. [54] found that the microstructure of low Cr cast steel was refined by adding different amounts of V and Ti. It was found that additions of Ti (from 0.1 to 0.5%) and V (up to 0.38%) refined the martensitic matrix and produced (V–Ti)C carbides which enhanced the hardness and augmented the wear properties of the aforementioned alloy. Seidu [55] determined that the un-inoculated iron is characterized by an increase in the proportion of cementite, and there are either slight or no graphite flakes in it (Fig. 24a). Figure 24b illustrates that with the addition of 0.1 wt% inoculants, an uneven distribution of deformed graphite flakes formed. When the inoculant addition augmented to 0.2 wt%, additional graphite flakes in a pearlitic medium were observed known as type D. Further, adding up of 0.3 wt% inoculants provided distinct graphite flakes consisting of varying sizes which were homogeneously distributed and haphazardly oriented. This type of graphite is typical of type A graphite. Seidu observed that the carbon equivalent value (CEV) increases with increased addition of inoculants.

Table 9 shows that with an increase in inoculants per cent, the mechanical properties (ultimate tensile strength, hardness) of the ferrous casting decrease, and also the CEV increases. Moreover, the author found that the degree of graphitization increases when the silicon content in GCI sample increases.

Morrogh and Williams [56] examined the effect of with and without the addition of inoculants Ce on the mechanical properties and microstructure of haematite pig iron. The mechanical properties were analysed in the form of two sets of bars, i.e. one is remelted pig iron containing carbon 3.77%, manganese 0.73, silicon 3.05%, phosphorus 0.039%, sulphur 0.023% and another is remelted pig iron with cerium addition of about 0.040%. The result is demonstrated in Table 10, and it is very clear that with the addition of Ce, the transverse rupture stress, tensile strength, hardness, impact strength and also the compression strength increased as compared to that of untreated cast iron. Figures 25 and 26 show the microstructure of untreated and cerium-treated remelted pig irons. Some combinations of undercooled as well as normal graphite flakes in the matrices of ferrite with some pearlite were found in the micro-images of all untreated bars, whereas all the treated bars demonstrated hypereutectic spherulitic structure collectively with quasi-flake graphite.
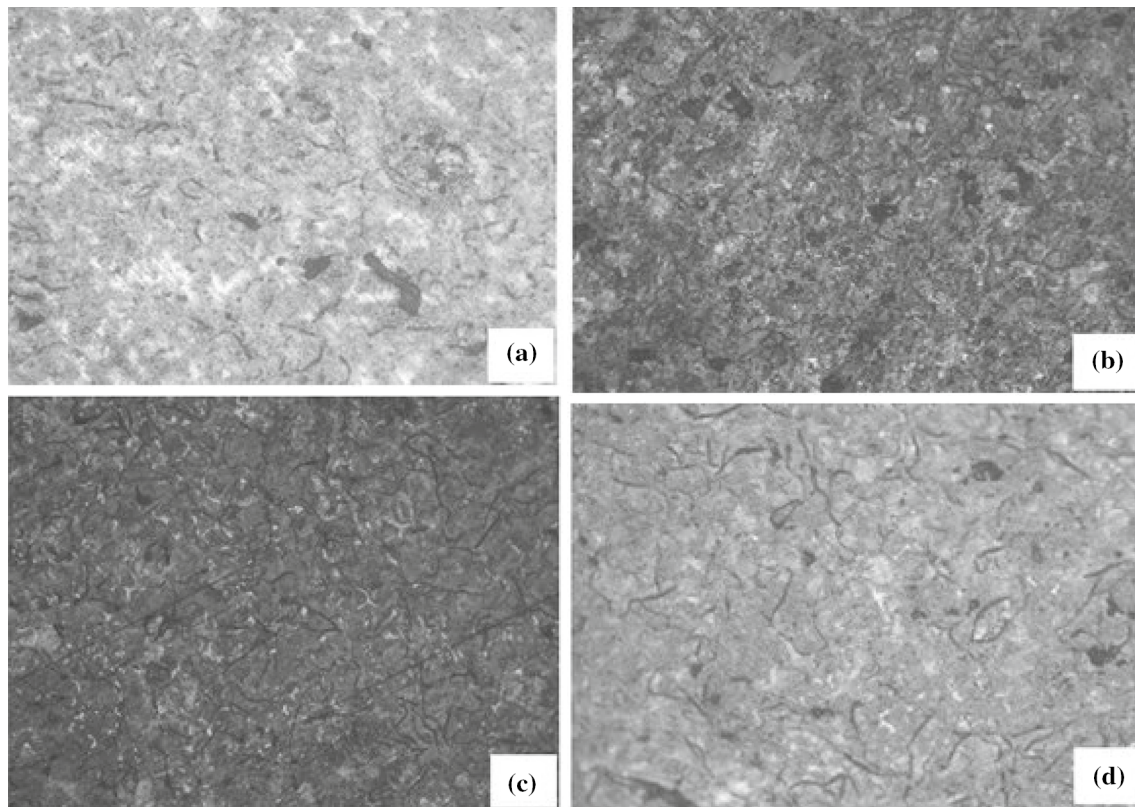
Fig. 24 Microstructure of **a** un-inoculated iron and varying inoculants addition from **b** 0.1 wt%, **c** 0.2 wt%, **c**, **d** 0.3 wt% [55]

| Table 9 Percentage of inoculants increase affects the mechanical properties [55]	% of FeSi added	Carbon equivalent value (CEV) = %C + %(Si + P)/(3)	Hardness (HRC)	Ultimate tensile strength (N/mm^2)
	Un-inoculated	3.507	58.9 ± 2.00	260.31
	0.1%	3.859	51.35 ± 0.73	238.43
	0.2%	3.953	45.88 ± 1.61	179.35
	0.3%	3.043	44.70 ± 2.77	142.15

Mangulkar and Borse [57] investigated the effect of inoculation (Fe–Si75 + RE Alloy) on the microstructure, hardness and tensile strength of GCI. The inoculant ferrosilicon (FeSi75) contains 73.47% Si, 0.76% Sr, 0.68% Ca and 0.23% Al, whereas rare-earth (RE) alloy contains 63.83% Ce and 34.52% lanthanum (La). Figure 27 shows the micrographs of the un-inoculated sample before etching and after etching with 3% nital solution. From Fig. 27, it is clearly visible that the substitution of inoculants in the alloy provides different graphite flakes of altering sizes consistently distributed and haphazardly oriented. This type of graphite is typical of type A graphite, which is frequently preferred for most engineering applications. Table 11 shows that the CEV increases with increase in the addition of inoculants. However, the mechanical properties such as tensile strength and the hardness decrease on increasing inoculant's amount beyond an optimal level. Hsu et al. [58] investigated the correlation between the microstructures and mechanical properties of ductile iron (DI) alloyed individually with 4% cobalt (Co) and 4% nickel (Ni), and they were referred to as alloy 1 and 2, respectively. It was found that the alloy 2 possessed better yield strength and tensile strength than the alloy 1. Also, the hardness of alloy 2 was more, as it contained the greatest volume fraction of pearlite. It is finally established that the hardness of the iron is chiefly reliant on the substitution of alloys and phase constituent present in the microstructure apart from the graphite morphology.

Ferrous alloys have widespread applications such as in structural engineering, making cooking utensils, engine blocks, foundation for large machineries and tools; from the above analysis on ferrous alloys, it is seen that the optimum

Table 10 Mechanical properties of unprocessed and Ce-processed cast irons [56]

Test bar diameter (in.)	Transverse rapture stress (p.s.i.)		Deflection (in.)		Tensile strength (p.s.i.)		BHN		Impact strength, ft.-lb.		Compression strength (p.s.i.)		Shear strength (p.s.i.)	
	W/O Ce	With Ce	W/O Ce	With Ce	W/O Ce	With Ce	W/O Ce	With Ce	W/O Ce	With Ce	W/O Ce	With Ce	W/O Ce	With Ce
1.6	51,500	99,000	0.20	0.32	25,100	55,050	154	186	–	–	71,600	127,100	–	–
1.2	64,500	101,500	0.28	0.38	32,050	55,500	160	198	–	–	–	–	36,500	49,700
0.875	68,870	105,4001	0.18	0.23	37,200	59,550	162	199	12	43	–	–	–	–
0.6	68,900	128,500	0.11	0.22	41,650	69,020	198	239	–	–	113,750	153,000	–	–
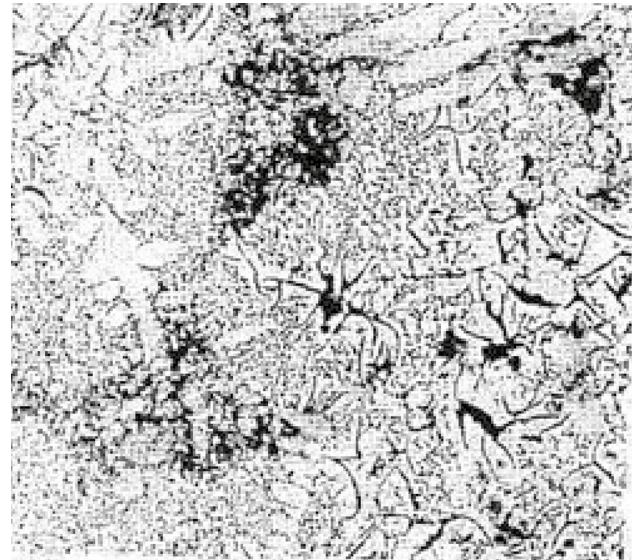
Fig. 25 Microstructure of untreated pig iron at ×100 magnification [56]
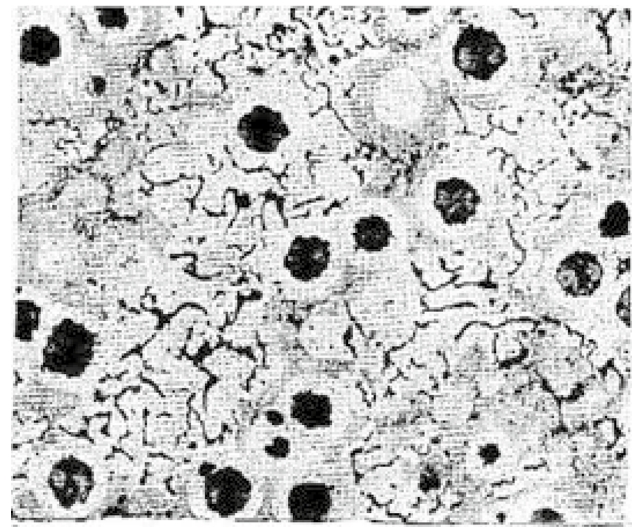
Fig. 26 Microstructure of cerium-treated remelted pig iron at ×100 magnification [56]

amount of addition of trace elements such as boron, bismuth, lead, titanium, cobalt, cerium and vanadium in ferrous alloys can significantly improve their microstructure and mechanical properties.

3.2 Non-ferrous Materials

Automotive sectors widely use aluminium–silicon (Al–Si) alloys owing to their fine castability, elevated strength-to-weight ratio, corrosion resistance and ease of recycling.
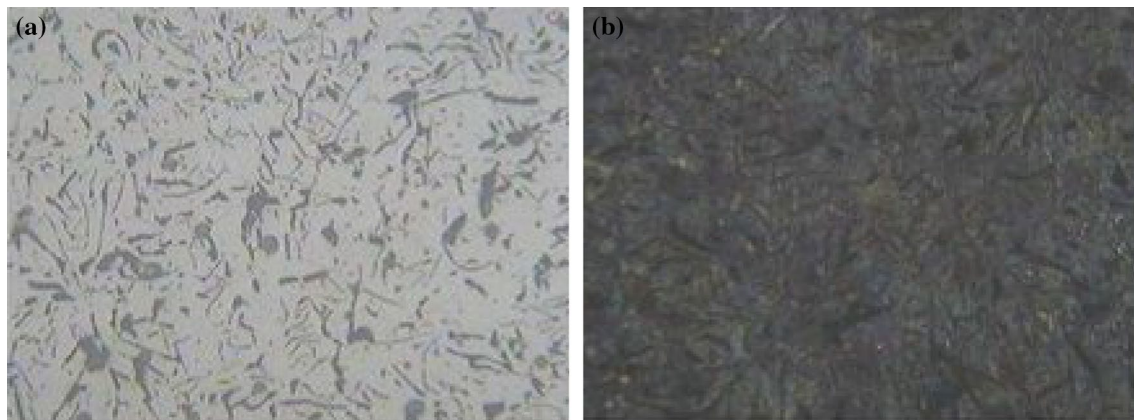
Fig. 27 Micrographs of **a** inoculated sample without etching; **b** inoculated sample after etching [57]

Table 11 Elemental composition and summary of the mechanical properties [57]

Element	C (wt%)	Si (wt%)	Mn (wt%)	P (wt%)	S (wt%)	Cr (wt%)	CEV (%)	BHN	UTS (N/mm^2)
Un-inoculated	3.56	2.12	0.68	0.1	0.083	0.08	4.244	229	227
Inoculated	3.5	2.51	0.59	0.201	0.053	0.07	4.325	187	202.68
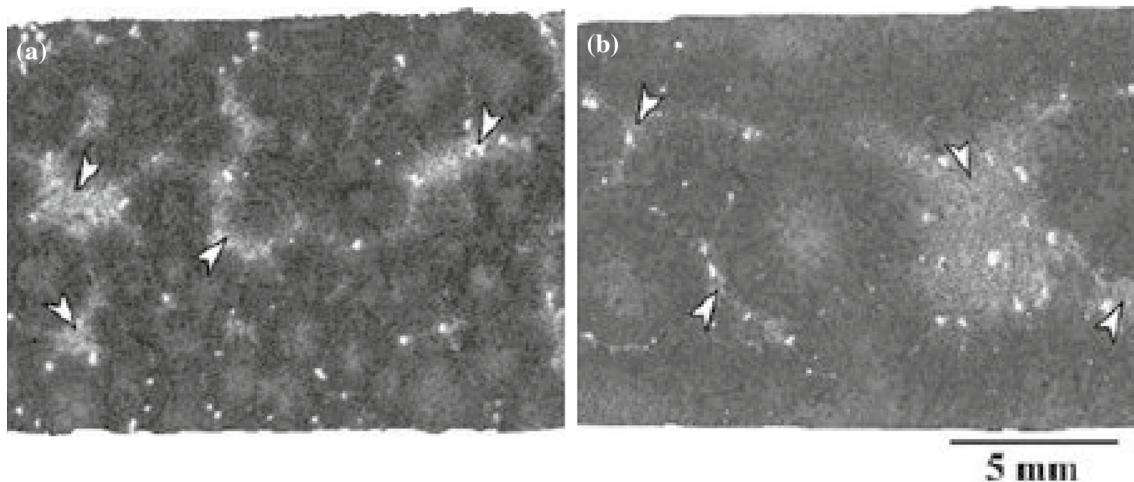
Fig. 28 Macrographs of Al-10% Si alloys modified by addition of **a** 140 ppm Sr; **b** 20 ppm Na [59]

Trace elements usually found in Al alloys significantly influence their mechanical properties as well as microstructures. Mcdonald et al. [59] investigated the effect of strontium (Sr) or sodium (Na) addition in hypoeutectic Al–Si alloys. Authors found that the substitution of Sr or Na led to increased porosity per cent in hypoeutectic Al–Si alloys owing to the creation of abundant, nearly spherical, detached and scattered pores as shown in Fig. 28. Researchers found that inclusion of Sr or Na extensively increased the eutectic grain size. It is indeed interesting to ascertain whether the increase in porosity can be primarily attributed to an increase in eutectic grain size.

Casari et al. [60] examined the effect of Ni and vanadium (V) addition on the impact strength of as-cast and T6-heated A356 alloy via sand casting. It was found that Ni exhibited a negligible effect on the impact strength of A356 alloy as compared to that obtained by addition of V. Vanadium in solid solution caused a substantial loss of ductility, which sequentially diminished the total absorbed energy due to the finer microstructure of permanent mould cast alloy. Further, the Casari et al. [61] investigated the influence of Ni and V on the mechanical properties of as-cast and T6-heated A356 alloy. Authors found that in as-cast condition, the formation of Ni-rich intermetallics robustly affected the tensile
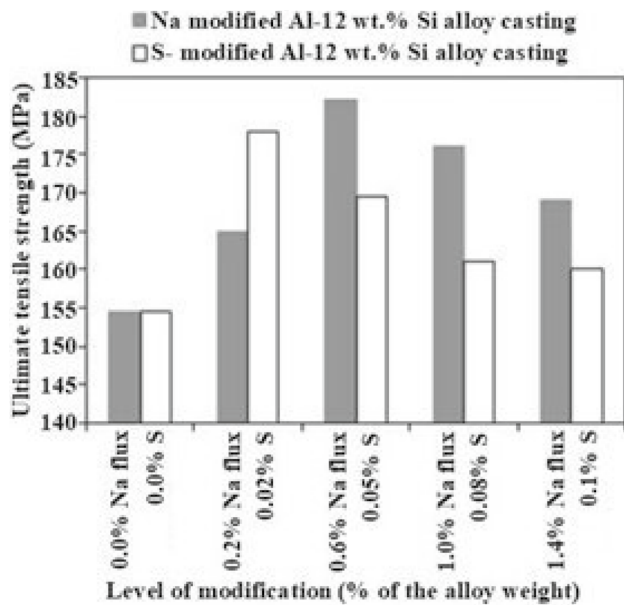
Fig. 29 Effect of modifier level on the UTS of eutectic Al–Si alloy [62]

Fig. 30 Deviation of UTS with different % of grain refiner [1]

properties of the sand-cast A356 alloy, causing a decline in both the yield strength (YS) and ultimate tensile strength (UTS), but the V addition enhanced the YS and UTS, owing to a solid solution strengthening effect. V-containing alloy post-T6-heat treatment showed somewhat increased mechanical properties as regards the A356 reference alloy, while the harmful effect of Ni was eradicated. In permanent mould casting, the A356 reference alloy and Ni or V-containing alloy showed no significant difference in mechanical properties in both as-cast and T6 condition because the cooling rate influences the mechanical characteristics of permanent mould casting.

Onyia et al. [62] studied the influence of sulphur (S) or sodium on the mechanical characteristics of sand-cast eutectic Al–Si alloy. The UTS of modified Al–Si alloy with different proportions of S or Na is shown in Fig. 29, and it is very clear that inoculation of the alloy with 0.6% and 1.0% Na resulted in highest UTS. However, high Na concentration beyond 1.0% decreased the mechanical properties of the aforementioned alloy. Addition of 0.02% and 0.05% of S to the eutectic Al–Si alloy led to an improvement in UTS. On the other hand, a rise in concentration of S beyond
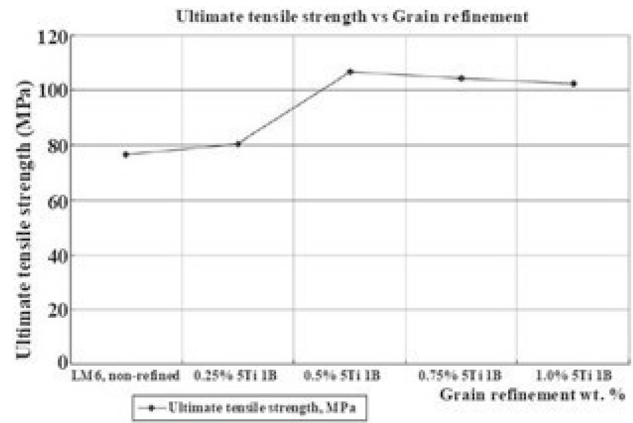
the optimal level (0.05%) fairly diminished the mechanical properties of the alloy due to a reduction in fineness of the eutectic Si. John [52] did grain refining of Al alloy by adding 0.2% of Ti or 0.02% B. which led to the reduction in grain size from 2.5 to 0.1 mm.

Ajibola et al. [63] inspected the effect of MgFeSi inoculant on properties of sand-cast 6061 Al alloy. The mechanical strength, hardness and the microstructure of the aluminium casting are usually improved by controlling the melting temperature, pouring temperature and the solidification process. It was found that the substitution of inoculant improved the solidified structure of cast alloy and, thus, improved the mechanical properties of the casting. From Table 12, it is evident that the increased amount of MgFeSi from 1 to 3% enhanced the mechanical properties because the number of pores was gradually decreased with the increase of 1 to 3% inoculants content.

In Al alloys, grain refinement is done by adding a precise amount of chosen grain refiners to inoculate the molten alloy. There is no rule to determine the best possible level of it to be inserted into the molten alloy for producing qualitative castings. Al–Ti–B master alloys are usually utilized as grain refiners in the Al–Si alloy castings to improve the grain structure. Pio et al. [1] examined the influence of grain refiner (Al_5Ti_1B) on the mechanical properties of the sand-cast (LM6) Al–Si alloy. Figure 30 shows the deviation of UTS with respect to different levels of grain refiner. It is seen that the unrefined LM6 had UTS of 76.73 MPa.

Table 12 Effects of varying percentages of inoculant on mechanical properties of cast Al alloy samples [63]

Sample	% MgFeSi	BHN Pnt 1	BHN Pnt 2	BHN Pnt 3	BHN Pnt 4	Average BHN	Strength (MPa)	Observation (porosity, etc.)
Cast-01	0	61.3	60.8	63.2	64.3	62.4	224.83	Cracks, pores
Cast-02	1	63.4	64.4	64.1	63.3	63.8	226.49	More pores
Cast-03	2	64.3	62.6	65.9	65.8	64.6	229.46	Fewer pores
Cast-04	3	61.4	71.2	69.4	60.8	65.7	237.14	Few pores
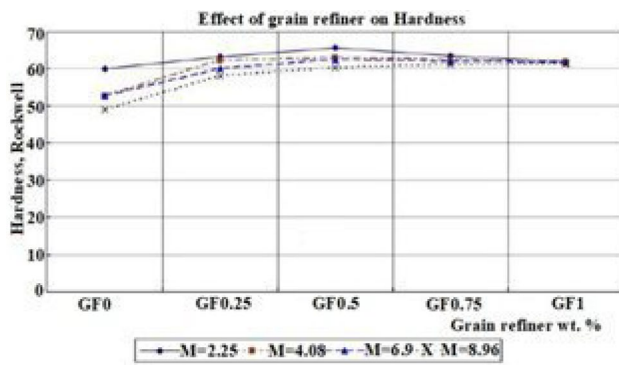
Fig. 31 Deviation of hardness with different % of grain refiner [1]

Fig. 34 Hardness versus casting condition [64]

Fig. 32 Micrographs of unrefined LM6 [1]

Fig. 35 Ultimate tensile strength versus casting condition [64]
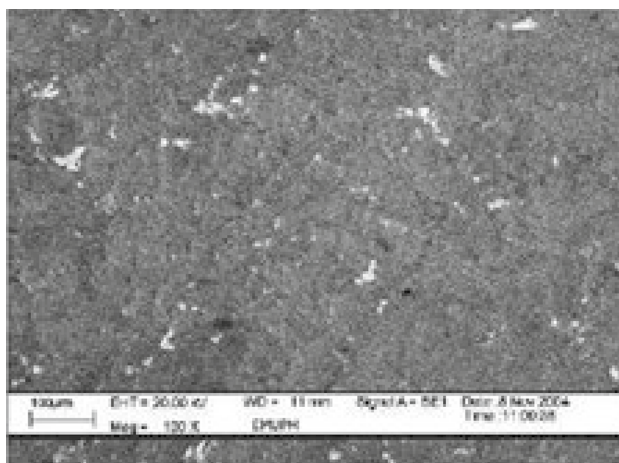

Fig. 33 Micrograph of 0.5 wt% Al5Ti1B refined LM6 [1]

However, the UTS was enhanced by 39% after the addition of 0.5 wt% Al_5Ti_1B grain refiner. It is further found that the mechanical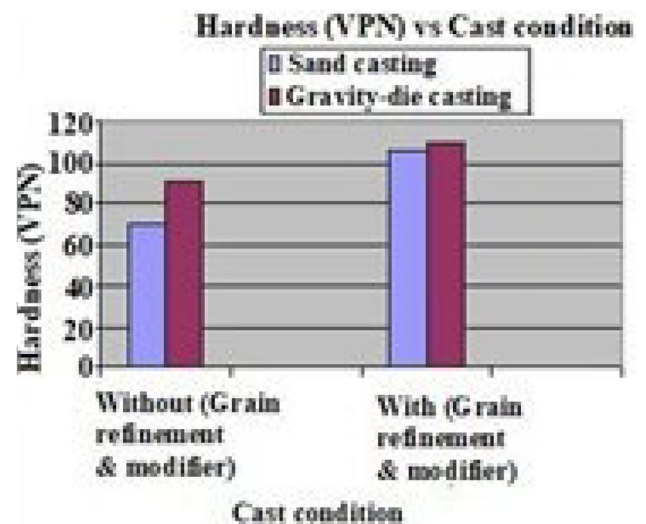 pr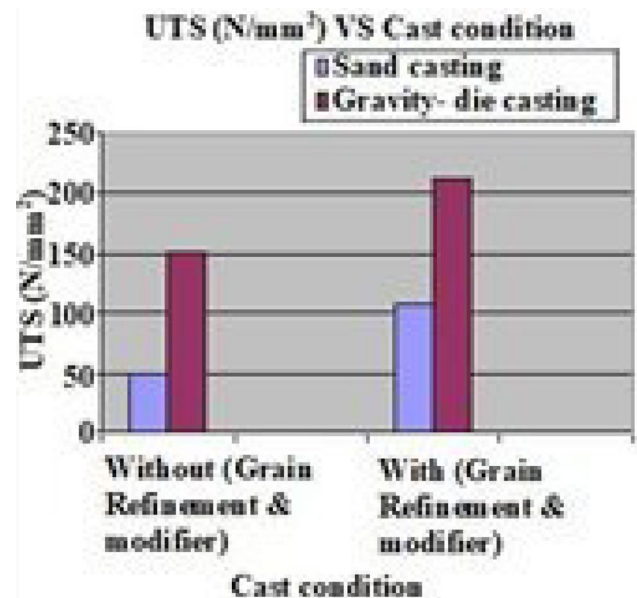operties of the casting did not increase with the addition of inoculants above 0.5 wt%. Figure 31 shows the highest hardness achieved in addition of 0.5 wt% grain refiner. The micrographs of unmodified and 0.5 wt% Al_5Ti_1B modified LM6 sand casting are depicted in Figs. 32 and 33. It is clearly seen that the grain structure became finer after inoculating the LM6 alloy with grain refiner.

Patel et al. [64] investigated the effect of grain refiner (Al–3Ti–1B + Al–10Sr) on the mechanical properties of sand casting and permanent die casting of Al–Si alloy. From Fig. 34, it is clearly visualized that the hardness enhanced by 51% (70 to 106 VPN) in sand casting and by 22% (90 to 110
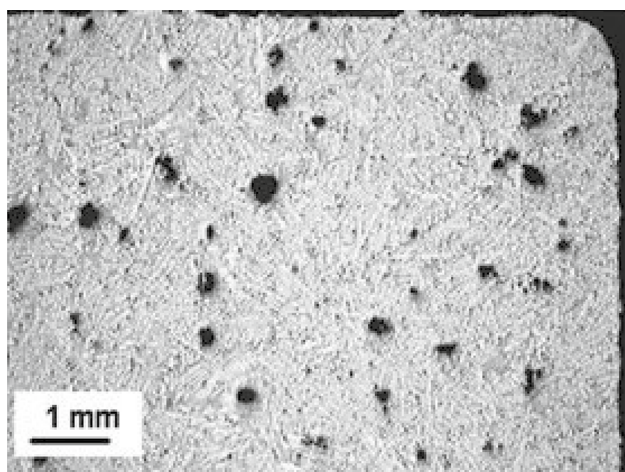
Fig. 36 Sand-cast specimen of worst quality having numerous pores [66]

Fig. 37 Fatigue fracture surface of a sand-cast sample showing initiation from a surface hollow [67]

Fig. 38 Fatigue fracture surface of a polished specimen showing initiation from a pore [67]

VPN) in case of permanent die casting. Figure 35 shows that the UTS increased by 118% (49 to 107 N/mm^2), and by only 40% (151 to 211 N/mm^2) in case of permanent die casting.

Wang [65] studied the tensile and fracture properties of A356/357 alloys, and it was found that the SDAS controlled the tensile properties and fracture behaviour of cast A356 and A357 alloys. The aforementioned alloys with Sr modification exhibited superior ductility (more for A356 alloy), but to some extent decreased the yield strength. With an increase in Mg content, the matrix strength and eutectic particle size increased. However, it diminished the ductility of both alloys (Sr-modified and unmodified). The aforementioned alloys with big and elongated particles demonstrated elevated strain hardening, and consequently possess increased damage accumulation rate due to particle cracking. Linder et al. [66] determined the effect of porosity on fatigue life of both permanent mould and sand-cast specimens (Fig. 36). The authors found that the fatigue strength reduced with a rise in pore fraction in both cases.

Jiang et al. [67] studied the fatigue performance of both die and sand-cast Al–7Si–Mg alloy. Figures 37 and 38 show the SEM image of the fatigue fracture surface of a sand-cast specimen showing crack initiation from both a hollow surface and a pore. It is seen that the crack growth at hollow sites is much higher than that at other sites. The stress concentration at hollow section was much higher than that at other defects which made it easy for the micro-cracks at those areas to initiate and grow. Authors concluded that the surface hollows dominated fatigue crack initiation and became the sole failure origins in sand-cast specimens with high surface roughness. The die-cast samples generally exhibited much lower porosity than the sand-cast samples due to faster solidification rate.
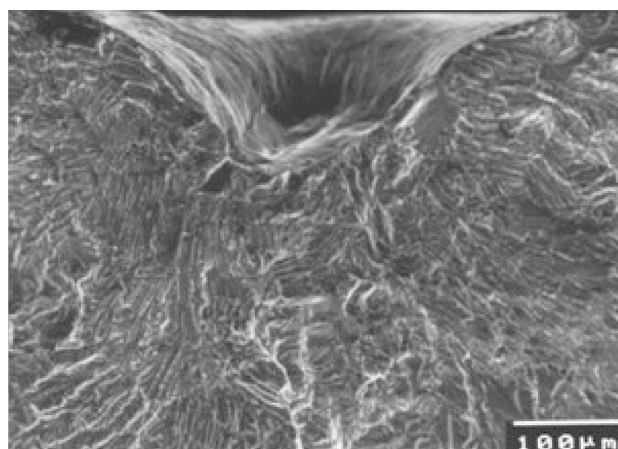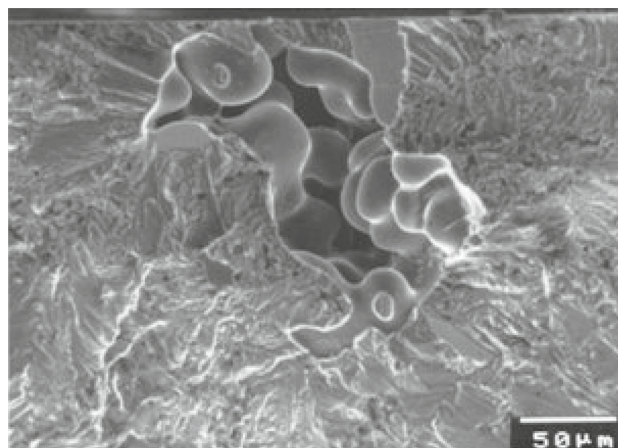
Ammar et al. [68] studied the influence of surface porosity on fatigue life of AE425 hypereutectic Al–Si sand-cast alloys at different temperatures, i.e. 150 °C and 300 °C. The authors found that the surface porosity is the chief crack initiation site, which led to the fracture of specimens (Figs. 39 and 40). It is clear that the surface porosity at the crack initiation site is either a single surface pore from which the crack extends or a sponge-like area having numerous pores at the crack site.

Liu et al. [69] prepared a new experimental alloy, i.e. Mg–5Zn–2.5Gd–0.4Zr by sand casting process which had a reasonable amount of gadolinium (Gd). The microstructure and mechanical properties of the prepared alloy were examined and judged with respect to the commercial ZK51A alloy. Figure 41a, b exhibits the micrographs of the cast aforementioned magnesium alloy, and it is very clear
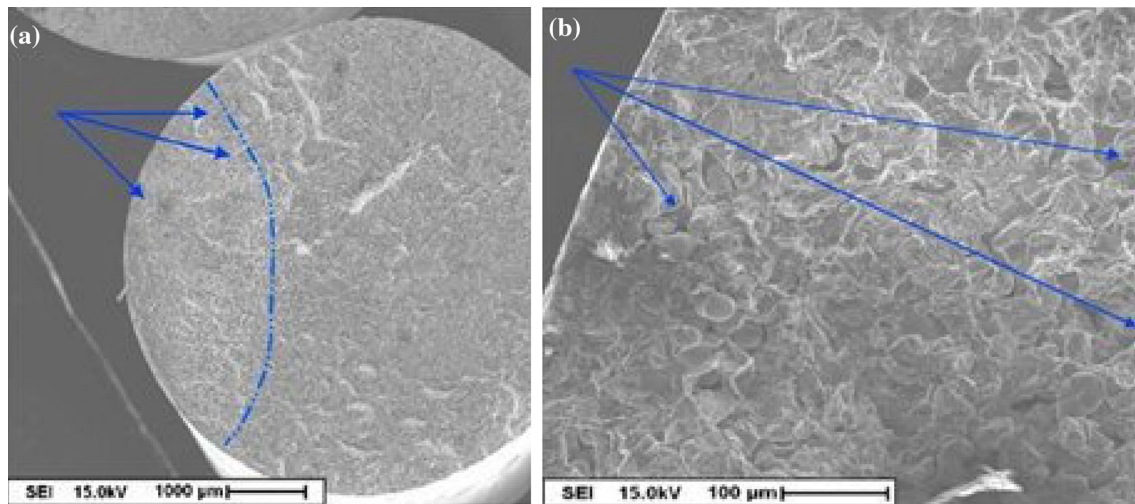
Fig. 39 SEM micrographs of the fatigue fracture surface of AE425 casting analysed at 150 °C, **a** at low magnification; **b** at high magnification [68]
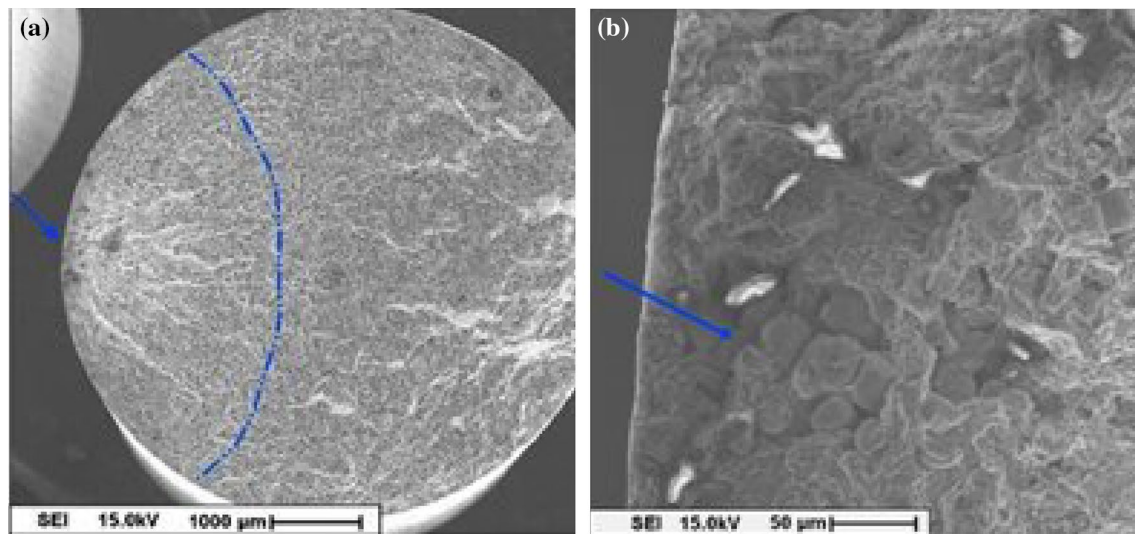

Fig. 40 SEM micrographs of the fatigue fracture surface of an AE425 casting analysed at 300 °C, **a** at low magnification; **b** at high magnification [68]

that the as-cast alloy possess equiaxed α-Mg grains, big-bone-like interdendritic α-Mg + W(Mg3Zn3Gd2) eutectic, Mg3Gd phase, icosahedral quasicrystalline I(Mg3Zn6Gd) and α-Zr particles. It was found that the alloy, when subjected to heat treatment, led to the disappearance of interdendritic particles, and the majority of eutectics turned to fine particle shape (Fig. 42). The mechanical properties of the as-cast prepared alloy, T4 treatment and T6 treatment at room temperature are displayed in Fig. 43. It is quite visible that the solution treatment led to a great increase in elongation, comparatively small rise in UTS and yield strength (YS) with respect to those obtained from the as-cast

specimen. However, further ageing treatment caused significant enhancement in UTS and YS with little decline in elongation. It is seen from Fig. 43 that UTS and YS at 200 °C of the prepared alloy are up to 145 MPa and 89 MPa, which are superior to those of ZK51A alloy.

Electromagnetic stirring (EMS), EMS and vibration, ultrasonic vibration, mechanical stirring and semi-solid metal forming methods are usually used in the semi-solid state so as to improve the mechanical properties of both ferrous and non-ferrous alloys. Hernandez et al. [70] determined the effect of EMS on microstructure refinement of the sand-cast 319Al–Si hypoeutectic alloy. Figure 44a, b shows
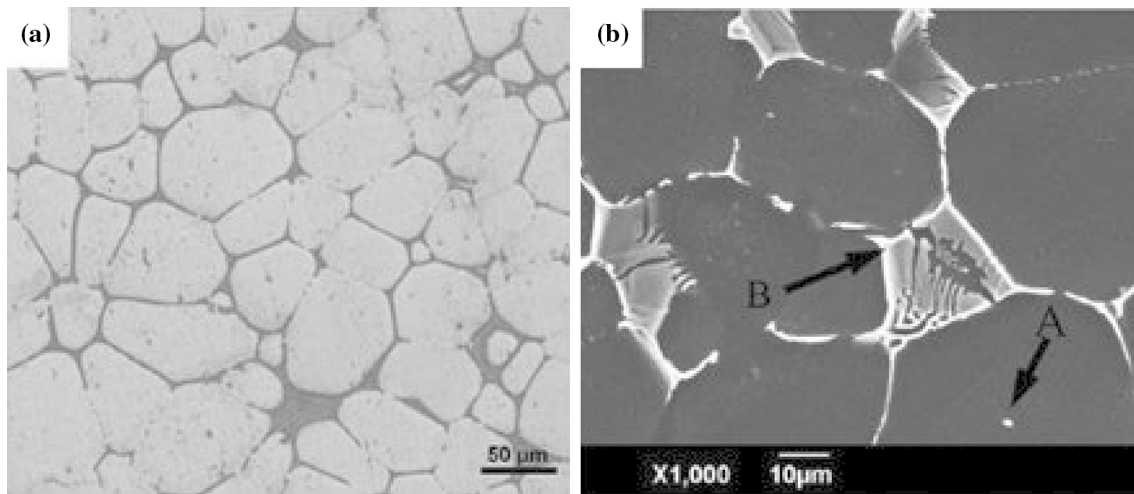
Fig. 41 Micrographs of the as-cast Mg–5Zn–2.5Gd–0.4Zr alloy, **a** OM image; **b** SEM image [69]
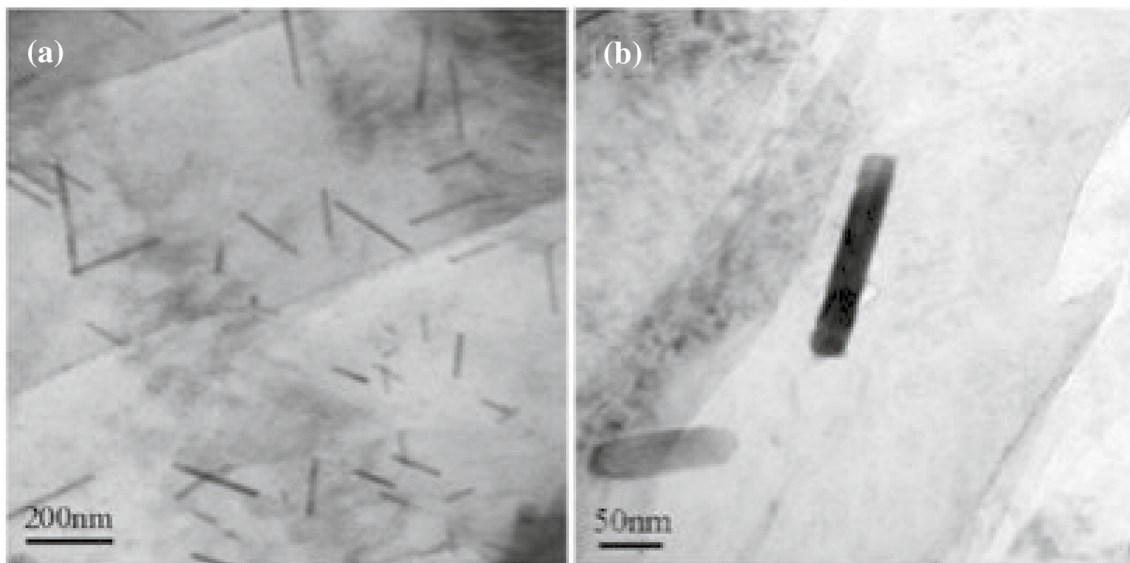

Fig. 42 TEM image of the long-rod-like precipitates in the solution-treated Mg–5Zn–2.5Gd–0.4Zr alloy at **a** low magnification; **b** high magnification [69]

the phases present in the microstructure of the aforementioned alloy at as-cast and EMS-treated (via an AC current of 8A) states. The main difference found amid the microstructures of as-cast and EMS-treated samples is the modification of dendrites to a semi globular structure at the latter case. On the other hand, the Si found in the Al–Si eutectic did not exhibit considerable modification.

Lu et al. [71] examined that effect of EMS on the morphology of primary Si particles (PSPs) in a hypereutectic Al–Si alloy. The graph of the equivalent diameter of PSPs at different stirring currents is shown in Fig. 45, and it is apparent that the size of PSP is minimum at the stirring current of

8A and PSPs congregated to form large chunks at high EMS current. Authors concluded that a weak EMS current is quite capable of refining PSPs, and the degree of congregation of PSPs is directly proportional to the square of stirring current.

Jin et al. [72] explored the microstructure and corrosion characteristics of mischmetal-modified AZ91D Mg alloy with and without EMS. The authors found that there was considerable amount of grain refinement and decrease in quantity of uneven-shaped β ($Mg_{17}Al_{12}$) phase on grain boundaries in case of EMS-treated casting. SEM micrograph of EMS-modified mischmetal inoculated AZ91D Mg alloy at various voltages is demonstrated in Fig. 46. It
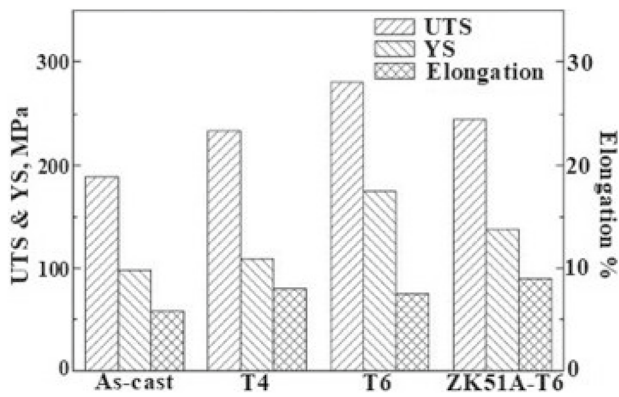
Fig. 43 Mechanical properties of the prepared alloy exhibiting different conditions at room temperature [69]
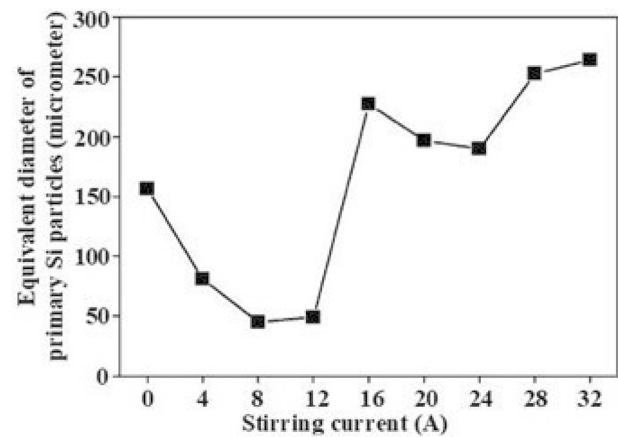

Fig. 45 Equivalent diameter of PSPs versus stirring current [71]

is apparent that there is no considerable reduction in the size of primary α-Mg grain at 50 V. However, the breakage of β ($Mg_{17}Al_{12}$) grain and increase in the volume fraction of Al_4(Ce, La) phase were observed. At 120 V, there is a great refinement in the microstructures of the alloy followed by an appreciable reduction in grain size owing to high intensity of stirring.

Liu et al. [73] explored the influence of Sr and EMS on the microstructure of AZ91 alloy. The as-cast microstructure was found to be refined on the addition of Sr content between 0.1 and 0.3 wt% in the aforementioned alloy; however, no new phases were visualized. It was found that the combined effect of Sr addition and EMS processing of the alloy not only reduced the grain size, but also altered the morphologies of the β ($Mg_{17}Al_{12}$) phases and decreased their volume percentage. The optimum quantity of Sr content in the alloy was found to be 0.2 wt%, as it led to the least grain size at both non-stirred and stirred

conditions. Additionally, the Brinell hardness (HB) value of the alloy at 0.2 wt% Sr was further enhanced with the exciting voltage of 100 V.

The alloy whose microstructures have been subjected to grain refinement possesses many advantages such as good mechanical properties thermal stability and high strain rate. The grain refinement can be attained either when external forces are applied to increase the fluid flow during solidification mechanical stirring or when electromagnetic stirring of melt. The use of mechanical vibration during pouring and solidification is one of the techniques to improve grain refinement of the cast alloy. Girija et al. [74] studied the effect of mechanical vibration on mechanical properties and microstructure of Al–Cu–Si alloy. Figure 47 shows the microstructure of Al–Cu–Si alloys with and without vibration at different frequencies. From Fig. 47f without vibration, the coarse grain structure owing to the existence of silicon flakes and intermetallic compounds of Cu and Al
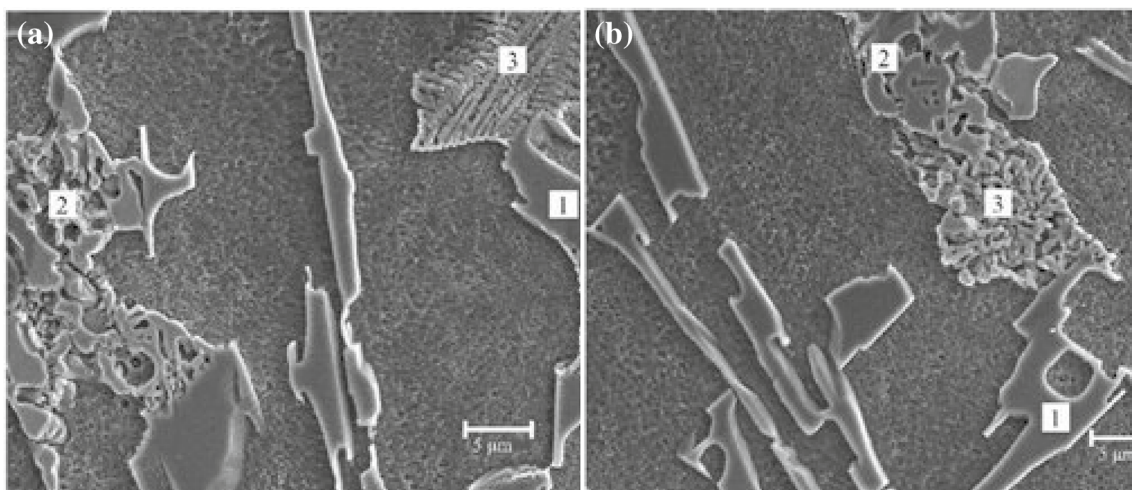
Fig. 44 SEM images of the 319 alloy samples, **a** as-cast; **b** EMS treated; 1, 2 and 3 denote Al–Si, Fe base and Cu-rich phases [70]
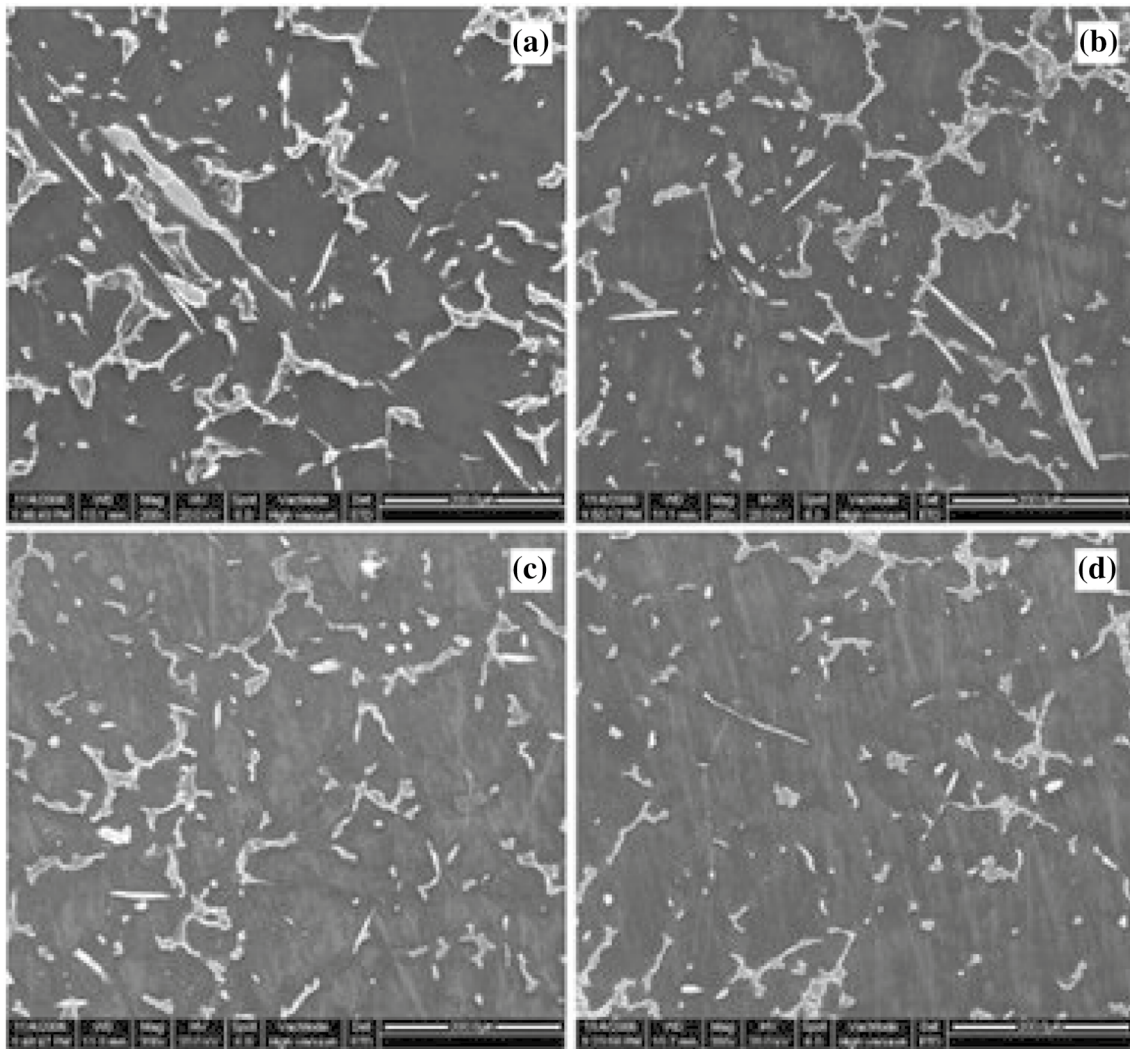
Fig. 46 SEM micrographs of EMS-modified mischmetal inoculated AZ91D Mg alloy at different voltages: **a** 0 V, **b** 50 V, **c** 80 V, **d** 120 V [72]

Fig. 47 OM of Al–Cu–Si alloy at ×300 magnification with frequency of **a** 50 Hz, **b** 40 Hz, **c** 30 Hz, **d** 20 Hz, **e** 10 Hz, **f** 0 Hz [74]
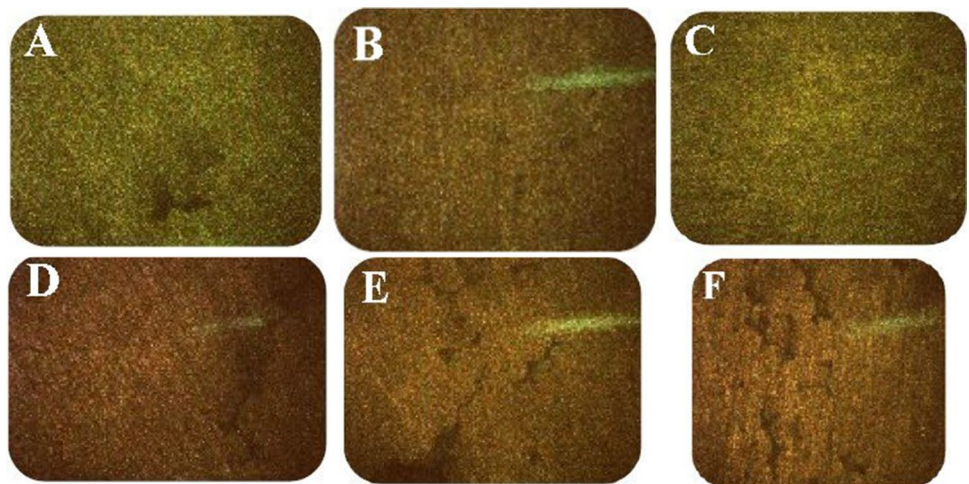
Table 13 Vibration conditions used for experimental mechanical properties obtained from casting sample [75]

Frequency	Amplitude	UTS (MPa)	YS (MPa)	Elongation (%)	Toughness (J)	Hardness (HV) at load 25 Gf for 30 s
0	0	158	115.6	3.6	2.5	60
100	5	177.5	127.4	4.5	3	66.7
200	5	182.6	135.4	4.8	4.5	72
300	5	200.5	138.7	5.5	6.5	79
400	5	216.08	140.5	7.5	8	85.8
100	10	174.5	125.5	4.2	3.5	69.8
200	10	176.4	130.5	4.35	3	72.5
300	10	188.6	132.5	5.8	5.5	75.5
400	10	208.47	136.8	6.5	6.5	81.9
100	15	165.2	122.4	3.78	4.5	65.6

is clearly seen. The microstructure of the alloy with vibration led to grain refinement and decreased the formation of intermetallic compounds of Cu and Al (Fig. 47a–e). Authors observed that the UTS, hardness and impact strength values increased with mechanical vibration as compared to without mechanical vibration and increases with an increase in frequency of mechanical vibration.

Kumar et al. [75] examined the influence of mechanical vibration parameters, namely frequency and amplitude, on the microstructure and mechanical properties of A356 alloy casting. The ranges of frequency and amplitude were 0–400 Hz and 0–15 μm. It is found from Table 13 that the UTS, YS, toughness and hardness are the maximum at frequency of 400 Hz and amplitude 5 μm. Authors observed that the UTS, YS and percentage elongations were improved by 26.8%, 17.7% and 52%, respectively, as compared to that of the casting prepared without vibration.

Abu-Dheir et al. [76] investigated the effect of mechanical vibration on the microstructure of eutectic Al–Si casting alloy operating at a frequency and variable amplitudes of 100 Hz and in the range of 18–199 μm. The minimum Si flake length and eutectic lamellar spacing were found to be 10.5 μm and 1.5 μm. Authors found that the range of amplitude of vibration strongly influenced the Si morphology, and with rise in vibration amplitude, silicon morphology became more fibrous and lamellar spacing reduced.

Finishing processes perhaps is used to enhance the wear resistance, corrosion resistance, hardness and control the surface friction. Fouad and Batanouny [77] investigated the influence of surface treatment on wear behaviour of Mg alloy AZ31. The surface treatments done on nine samples at pressure load condition of 0.1 and 0.3 bar were ball burnishing, swaging and shot peening. It was found that shot-peening samples showed the worst wear rate as compared to other samples at 0.1 bar, whereas the cast samples exhibited worst wear rates at pressure load 0.3 bar. Alternatively, the hardness value of the swaged sample was found to be the highest as compared to the other samples.

Among non-ferrous alloys, Al alloys are most widely used. The commonly employed grain refiners to refine primary (α)-Al are Al–10Ti, Al–5Ti–1B, etc. The trace elements, namely strontium, sodium, sulphur, etc., are used to improve the microstructure and mechanical properties of the cast alloy. However, there is an optimum limit of the addition of grain refiners as well as trace elements to the alloy which needs to be identified; otherwise over-modification of the microstructure may be detrimental to the casting's mechanical properties. Mechanical vibrations and EMS processing of the alloy further improve the quality of the cast part.

4 Metal Matrix Composite (MMC) Via Sand Casting

MMC contains at least two basic parts, out of which one is essentially a metal, while the other part may be a different metal or another material such as ceramic or organic compound. When MMC is composed of at least three different materials, it is known as hybrid composite. Being light weight, MMCs are employed in spacecraft, helicopters and aircraft. The main advantages of MMCs are their enhanced mechanical and physical properties such as strength, stiffness and hardness with regard to the base material [78, 79]. Researchers have used many casting methods such as sand casting, die casting and squeeze casting to prepare MMCs. However, this section includes the studies on MMCs prepared via sand casting route.

Fernández et al. [80] prepared A356 Al alloy using cylindrical sand moulds, and afterwards, the cylindrical specimens were atomized by rotating electrode process (REP). Alpha silicon nitride (Si_3N_4) with diverse weight per cents of 10, 20 and 30% was substituted to the alloy powder using a planetary ball mill to produce A356–Si_3N_4 composites. It was found that the microstructure homogenized and nanoscale crystallites formed at shorter milling times.

Longer milling times augmented the dislocation density which is beneficial for sequential sintering.

Roseline and Paramasivam [81] manufactured Al composites reinforced with Fused Zirconia Alumina 40 (FZA40) of varying vol% of 0, 5, 10 and 15% by double-stir casting route. Eight castings were produced using sand moulds. Out of which, four samples were heat-treated at 250 °C for a period of 1 h, and then they were cooled at ambient condition. The casting samples were subjected to the microhardness test and corrosion (static immersion and electrochemical) test. It was found that with an increase in vol% of reinforcement in the Al matrix, the hardness of the MMCs increased considerably. The rise in hardness was attributed to a huge increase in the number of dislocations created at the particle–matrix interface during the solidification stage. The heat-treated MMCs also exhibited a huge increase in hardness value due to the occurrence of hard reinforcement particle Al_3Zr on the surface which resisted the plastic deformation of the MMCs. The untreated and treated reinforced MMCs displayed better corrosion resistance as compared to unreinforced alloy. It may be due to the occurrence of alumina and Al_3Zr phases on the surface which would have prohibited the sulphide molecules (from H_2SO_4 treatment) to invade into the intergranular spaces of the MMCs, thus averting the composite from undergoing corrosion.

Fayomi et al. [82] investigated the effect of ZrB_2–Si_3N_4 of varying vol% of 5, 10, 15 and 20% on the properties of AA8011 MMC prepared by two-step stir casting route. The properties of the MMCs inspected were UTS, YS, hardness, electrical conductivity and resistivity. It was found that the mechanical properties, i.e. UTS, YS and hardness of the developed composite, increased with increase in vol% of hybrid particulates. The reason behind is that there was a uniform distribution of ZrB_2–Si_3N_4 particulates in AA8011 matrix which increased the load bearing capacity of MMCs, and also improved the intermetallic bonding with AA8011 alloy owing to complete wettability. It was further found that the electrical resistivity of AA8011 MMC was also enhanced with increase in the volume fraction of ceramic particulates. However, the electrical conductivity was found to be severely decreased. It occurred due to low conductive characteristics of the hybrid particulates and the minor porosity that had arisen in the MMCs during the manufacturing process.

Mkpume et al. [83] explored the physical, mechanical and morphological characteristics of silica sand reinforced Al composite. The mean particle size of silica sand used for the manufacture of MMC was −53 μm, and wt% substituted in Al matrix was 3, 7, 11, 15 and 19%. XRD analysis of the silica sand showed a higher per cent of quartz in it which indicates that it could be a fine strengthener. It was found that the density of the MMC exhibited a declining trend with an increase in wt% of silica sand. It happened because silica sand possesses lower density than Al, and it was found by the researchers [84, 85] that the MMCs possess lower densities as compared to monolithic metals and alloys. The hardness of the MMCs exhibited an increasing trend with respect to silica wt%. It may be due to hard silica sand particles in Al matrix which reduces the distortion of MMCs. The UTS of MMCs was found to increase by 32% by substitution of 11 wt% silica, and beyond 11%, there was a drop in strength. It may be due to good interfacial bonding between the matrix and the silica particles at threshold limit of reinforced material. However, increased per cent of silica enhances the porosity in MMC which acts as crack initiation site and, thus, decreases the load bearing capacity of the MMCs. Impact energy was found to increase up to 7 wt% silica content, and thereafter it decreased. It happened because the matrix could diffuse the load uniformly at and below 7 wt% silica, so that the MMCs could absorb more energy before fracture. Beyond this limit, the sharp edge of silica particles behaves as stress concentration point due to which crack occurs in the matrix, thereby causing a reduction in impact energy of the MMCs.

From the above literature survey on MMCs via sand casting process, it can be inferred that the reinforcing material should be evenly distributed within the metal/alloy as a matrix for achieving better mechanical properties of the developed MMCs. Heat treatment process refines the grain structure and improves the hardness of the composites. Care should be taken while preparing MMCs so that pores are as minimum as possible because these pores create a site for crack initiation, which adversely affects the load bearing capacity of the MMCs. The electrical conductivity of the composite is found to decrease by the substitution of nonmetallic particulates in matrix (metal) because of the low conductive characteristic of the reinforcing material. The density of the MMCs decreases with increased wt% of low-density reinforcing material.

5 Summary and Future Scope/Trends

On the basis of the present review, the following conclusions are drawn:

- The sand mould properties and their processing conditions to a great extent influence the mechanical properties of sand-cast parts.
- Morphological properties of the sand and binding mechanism occurring in the sand have a strong impact on the sand mould characteristics.
- Different additives, e.g. coconut shell powder, fly ash, tamarind powder, sodium carbonate, iron dust, molasses, starch powder, coal dust, etc., can be used to enhance

mould properties such as compressive strength, shear strength, collapsibility, permeability and hardness.

- Cheaper cost with uncompromised quality is the main concern of any production unit. The current state of the art indicates that there are various types of silica sands available at nearby areas close to foundry industries that, when mixed with few additives in adequate amounts, can be successfully used for casting both ferrous and non-ferrous castings.

- Three-dimensional printing process, used for preparing the sand casting mould, is quite a new area of research compared to the other available technologies, e.g. selective laser sintering (SLS) and stereolithography (SLA). The process is comparatively faster, more accurate, provides better surface finish and involves low cost.

- Trace elements are usually added in very small proportions to the alloy for improving their microstructures as well as increasing their mechanical and wear properties. Trace elements which are added to (a) ferrous alloys are: boron, bismuth, lead, titanium, cerium, vanadium, phosphorus and magnesium; (b) non-ferrous alloys are: strontium, sodium, nickel, vanadium, sulphur, titanium and boron. If hybrid sand casting processes such as EMS, vibration, and EMS and vibration are used along with the sand casting process, it would lead to further improvement in mechanical properties of the cast alloy.

- The effect of addition of various nano-compounds in the cast alloy may be investigated for achieving excellent mechanical properties for high-temperature applications.

- Substitution of reinforcing particulates such as ZrB_2–Si_3N_4, fused zirconia alumina, Si_3N_4 and silica sand in metal as matrix leads to improvement in mechanical properties as well as electrical diffusivity properties of developed MMCs.

References

1. Pio, L.Y.; Sulaiman, S.; Hamouda, A.M.; Ahmad, M.M.H.M.: Grain refinement of LM6 Al–Si alloy sand castings to enhance mechanical properties. J. Mater. Process. Technol. **162–163**, 435–441 (2005)
2. Kalpakjian, S.; Schmid, S.: Manufacturing Processes for Engineering Materials, 5th edn. Pearson Education Incorporation, London (2008)
3. Rao, P.N.; Lerner, Y.; Kouznetsov, V.: Rapid prototyping applications in metal casting. Inst. Eng. Malays. **64**(3), 1–7 (2003)
4. Jain, P.; Kuthe, A.M.: Feasibility study of manufacturing using rapid prototyping: FDM approach. Procedia Eng. **63**, 4–11 (2013)
5. Kundu, R.R.; Lahiri, B.N.: Study and statistical modelling of green sand mould properties using RSM. Int. J. Mater. Prod. Technol. **31**, 143–158 (2008)
6. Olasupo, O.A.; Omotoyinbo, J.A.: Moulding properties of a Nigerian silica-clay mixture for foundry use. Appl. Clay Sci. **45**, 244–247 (2009)
7. Ademoh, N.A.: Evaluation of the foundry properties of river Niger sand behind Ajaokuta steel company limited, Ajaokuta, Nigeria. Am. Eurasian J. Sci. Res. **3**, 75–83 (2008)
8. Lanre, S.Y.; Olumodeji, J.O.: Analysis of Ilorin sand moulding properties for foundry applications. Int. J. Eng. Res. Technol. **3**, 1520–1525 (2014)
9. Fo, E.; Ju, O.; Ee, N.: Effect of Ukpor clay content on the properties of synthetic moulding sand. Int. J. Res. Adv. Eng. Technol. **1**, 12–16 (2015)
10. Saikaew, C.; Wiengwiset, S.: Optimization of moulding sand composition for quality improvement of iron castings. Appl. Clay Sci. **67**, 26–31 (2012)
11. Chavan, T.K.; Nanjundaswamy, H.M.: Effect of variation of different additives on green sand mould properties for olivine sand. Int. J. Res. Adv. Eng. Technol. **1**, 1–4 (2013)
12. Seidu, O.S.; Kutelu, B.J.: Effects of additives on some selected properties of base sand. J. Miner. Mater. Charact. Eng. **2**, 507–512 (2014)
13. Loto, C.A.; Adebayo, H.: Effect of variation in water content, clay fraction and sodium carbonate additions on the synthetic moulding properties of Igbokoda clay and silica sand. Appl. Clay Sci. **5**, 165–181 (1990)
14. Rao, P.S.; Birru, A.K.: Effect of mechanical properties with addition of molasses and Flyash in green sand moulding. Mater. Today **4**, 1186–1192 (2017)
15. Kumar, S.; Gandotra, S.; Kumar, S.; Nripjit; Tripathi, H.: Investigate the effect of additives on mechanical properties during casting of 6351 aluminium. In: MATEC Web of Conferences 57 (2016). https://doi.org/10.1051/matecconf/20165703008
16. Okonji, P.C.; Nwobi-Okoye, C.C.; Atanmo, P.N.: Experimental study of the feasibility of using groundnut shell ash and ant hill powder in foundry application. J. Chin. Adv. Mater. Soc. (2018). https://doi.org/10.1080/22243682
17. Khandelwal, H.; Ravi, B.: Effect of moulding parameters on chemically bonded sand mould properties. J. Manuf. Process. **22**, 127–133 (2016)
18. Orumwense, F.F.O.: Moulding properties of synthetic sand mixtures—a comparative study. Scand. J. Metall. **31**, 100–106 (2002)
19. Lidumnieks, K.; Svidro, J.T.; Dioszegi, A.: The effect of various production parameters on the heat absorbing capacity of greensand. Int. J. Cast Met. Res. (2017). https://doi.org/10.1080/13640461.2017.1348005
20. Parappagoudar, M.B.; Pratihar, D.K.; Datta, G.L.: Linear and non-linear statistical modelling of green sand mould system. Int. J. Cast Met. Res. (2007). https://doi.org/10.1179/136404607X184952
21. Karunakar, D.B.; Datta, G.L.: Controlling green sand mould properties using artificial neural networks and genetic algorithms—a comparison. Appl. Clay Sci. **37**, 58–66 (2007)
22. Babu, N.N.; Ohdar, R.K.; Pushp, P.T.: Evaluation of green compressive strength of clay bonded moulding sand mix: neural network and neuro-fuzzy based approaches. Int. J. Cast Met. Res. **19**, 110–115 (2006)
23. Singha, S.K.; Singh, S.J.: Analysis and optimization of sand casting defects with help of artificial neural network. Int. J. Res. Eng. Technol. **4**, 24–29 (2015)
24. Guharaja, S.; Haq, A.N.; Karuppannan, K.M.: Optimization of green sand casting process parameters by using Taguchi's method. Int. J. Adv. Manuf. Technol. **30**, 1040–1048 (2006)
25. Upadhye, R.A.; Keshwani, I.P.: Optimization of sand casting process parameter using Taguchi method in foundry. Int. J. Res. Eng. Technol. **1**, 1–9 (2012)

26. Kumar, S.; Satsangi, P.S.; Prajapati, D.R.: Optimization of green sand casting process parameters of a foundry by using Taguchi's method. Int. J. Adv. Manuf. Technol. **55**, 23–34 (2011)

27. Surekha, B.; Kaushik, L.K.; Panduy, A.K.; Vundavilli, P.R.; Parappagoudar, M.B.: Multi-objective optimization of green sand mould system using evolutionary algorithms. Int. J. Adv. Manuf. Technol. **58**, 9–17 (2012)

28. Sachs, E.; Cima, M.; Cornie, J.; Brancazio, D.: Dimensional printing: rapid tooling and prototypes directly from CAD representation. In: International Solid Freeform Fabrication Symposium, pp. 27–47 (1990). https://doi.org/10.1016/s0007-8506(07)61035-X

29. Travitzky, N.; Bonet, A.; Dermeik, B.; Fey, T.; Filbert-Demut, I.; Schlier, L.: Additive manufacturing of ceramic-based materials. Adv. Eng. Mater. **16**, 729–754 (2014). https://doi.org/10.1002/adem.201400097

30. Singamneni, S.; Diegel, O.: Some recent developments and experiences with rapid manufacturing by indirect means. Asian Int. J. Sci. Technol. Prod. Manuf. Eng. **3**, 7–14 (2010)

31. Snelling, D.; Li, Q.; Meisel, N.; Williams, C.B.; Batra, R.C.; Druschitz, A.P.: Lightweight metal cellular structures fabricated via 3D printing of sand cast moulds. Adv. Eng. Mater. **17**, 923–932 (2015). https://doi.org/10.1002/adem.201400524

32. Dimitrov, D.; Schreve, K.; Beer, N.; Chritiane, P.: Three dimensional printing in the South African industrial environment. S. Afr. J. Ind. Eng. **19**, 195–213 (2008)

33. Dimitrov, D.; Schreve, K.; Beer, N.: Advances in three dimensional printing—state of the art and future perspectives. Rapid Prototyp. J. **12**(3), 136–147 (2006)

34. Ian, C.; David, B.; Ian, G.: Additive manufacturing: rapid prototyping comes of age. Rapid Prototyp. J. **18**(4), 255–258 (2012)

35. Peilan, Z.; Zhifeng, X.; Huan, Y.: Progress of rapid technology without mould in precision sand casting. Spec. Cast. Nonferrous Alloys **33**, 136–140 (2013)

36. Xu, Z.; Luo, J.; Song, X.: Study on measures to strengthen toughen precoated phenolic resin sand. Foundry **49**(6), 356–358 (2000)

37. Guo, Z.; Shan, Z.; Du, D.; Zhao, M.; Zhang, M.: Experimental investigation on the flow properties of sand granules in the process of sand mould printing. Rapid Prototyp. J. (2018). https://doi.org/10.1108/RPJ-04-2017-0065

38. Hawaldar, N.; Zhang, J.: A comparative study of fabrication of sand casting mould using additive manufacturing and conventional process. Int. J. Adv. Manuf. Technol. (2018). https://doi.org/10.1007/s00170-018-2020-z

39. Vaezi, M.; Chua, C.K.: Effects of layer thickness and binder saturation level parameters on 3D printing process. Int. J. Adv. Manuf. Technol. **53**, 275–284 (2011)

40. Snelling, D.; Blount, H.; Forman, C.; Ramsburg, K.; Wentzel, A.; Williams, C.: The effects of 3D printed moulds on metal castings. In: Proceedings of the Solid Freeform Fabrication Symposium, Austin, TX, pp. 827–45 (2013)

41. Koltygin, A.V.; Bazhenov, V.E.: Development of a substitute for Z cast moulding sand used on installations of 3D printing for obtaining aluminum, magnesium, and iron casting. Russ. J. Non-Ferrous Met. **53**, 38–41 (2012)

42. Coniglio, N.; Sivarupan, T.; Mansori, M.E.: Investigation of process parameter effect on anisotropic properties of 3D printed sand moulds. Int. J. Adv. Manuf. Technol. (2017). https://doi.org/10.1007/s00170-017-0861-5

43. Shifeng, W.; Qiwen, S.; Qingsong, W.: Material optimization and post-processing of sand moulds manufactured by the selective laser sintering of binder-coated Al_2O_3 sands. J. Mater. Process. Technol. **225**, 93–102 (2015)

44. Zhao, S.; Yao, S.; Yang, T.: Influence of resin flow on shrinkage of additive manufacturing coated sand moulds. China Foundry Res. Dev. **15**(4), 291–298 (2018)

45. Mitra, S.; Castro, A.R.D.; Mansori, M.E.: The effect of ageing process on three-point bending strength and permeability of 3D printed sand moulds. Int. J. Adv. Manuf. Technol. (2018). https://doi.org/10.1007/s00170-018-2024-8

46. Sivarupan, T.; Mansori, M.E.; Daly, K.; Mavrogordato, M.N.; Pierron, F.: Characterisation of 3D printed sand moulds using micro-focus X-ray computed tomography. Rapid Prototyp. J. (2018). https://doi.org/10.1108/RPJ-04-2018-0091

47. Fallon, M.J.: The effect of some trace elements in cast iron. Indian Foundry J. **26**, 1–12 (1980)

48. Ankamma, K.: Effect of trace elements (Boron and Lead) on the properties of gray cast iron. J. Inst. Eng. India Ser. D **95**(1), 19–26 (2014)

49. Shy, Y.; Hsu, C.; Lee, S.; Hou, C.: Effect of titanium addition and section size on microstructure and mechanical properties of compacted graphite cast iron. Mater. Sci. Eng. A **278**, 54–60 (2000)

50. Collini, L.; Nicoletto, G.; Konecna, R.: Microstructure and mechanical properties of pearlitic gray cast iron. Mater. Sci. Eng. A **488**, 529–539 (2008)

51. Behnam, M.M.J.; Davami, P.; Varahram, N.: Effect of cooling rate on and mechanical properties of gray cast iron. Mater. Sci. Eng. A **528**, 583–588 (2010)

52. John, K.C.: Metal Casting and Joining. Eastern Economy Edition. PHI Learning Private Limited, New Delhi (2015)

53. Qu, Y.; Xing, J.; Zhi, X.; Peng, J.; Fu, H.: Effect of cerium on the as-cast microstructure of a hypereutectic high chromium cast iron. Mater. Lett. **62**, 3024–3027 (2008)

54. Ruiz, S.I.M.; Gonzalez, P.O.; Hernandez, V.H.B.; Jacuinde, A.B.; Rodriguez, M.A.L.H.: Effect of V–Ti on the microstructure and abrasive wear behaviour of 6CrC cast steel mill balls. J. Miner. Mater. Charact. Eng. **2**, 383–391 (2014)

55. Seidu, S.O.: Effect of compositional changes on the mechanical behaviour of grey cast iron. J. Metall. Eng. **3**, 92–95 (2014)

56. Morrogh, H.; Williams, W.J.: The production of nodular graphite structures in cast iron. J. Iron Steel Inst. **150**, 306 (1949)

57. Mangulkar, Y.E.; Borse, S.C.: Effect of addition of inoculants on mechanical properties & wear behaviour of grey cast iron. Int. J. Innov. Res. Sci. Eng. Technol. **5**, 1131–1139 (2016)

58. Hsu, C.H.; Chen, M.L.; Hu, C.J.: Microstructure and mechanical properties of 4% cobalt and nickel alloyed ductile irons. Mater. Sci. Eng. A **444**, 339–346 (2007)

59. Mcdonald, S.D.; Dahle, A.K.; Taylor, J.A.; Stjohn, D.H.: Modification-related porosity formation in hypoeutectic aluminum-silicon alloys. Metall. Mater. Trans. **35**, 1097 (2003)

60. Casari, D.; Ludwig, T.H.; Garagnani, G.L.: Impact behaviour of A356 foundry alloys in the presence of trace elements Ni and V. J. Mater. Eng. Perform. **24**, 894–908 (2014)

61. Casari, D.; Ludwig, T.H.; Garagnani, G.L.: The effect of Ni and V trace elements on the mechanical properties of A356 aluminium foundry alloy in as-cast and T6 heat treated conditions. Mater. Sci. Eng. A **610**, 414–426 (2015)

62. Onyia, C.W.; Okorie, B.A.; Neife, S.I.; Obayi, C.S.: Structural modification of sand cast eutectic Al–Si alloys with sulfur/sodium and its effect on mechanical properties. World J. Eng. Technol. **1**, 9–16 (2013)

63. Ajibola, O.O.; Oloruntoba, D.T.: Effect of MgFeFi inoculant on properties of cast 6061 Al alloy for brake master piston application. Indian J. Mater. Sci. (2015). https://doi.org/10.1155/2015/756219

64. Patel, V.P.; Prajapati, H.R.: Microstructural and mechanical properties of eutectic Al–Si alloy with grain refined and modified using gravity-die and sand casting. Int. J. Eng. Res. Appl. **2**, 147–150 (2012)

65. Wang, Q.G.: Microstructural effects on the tensile and fracture behaviour of aluminum casting alloys A356/357. Metall. Mater. Trans. A **34**, 2887 (2003)

66. Linder, J.; Axelsson, M.; Nilsson, H.: The influence of porosity on the fatigue life for sand and permanent mould cast aluminium. Int. J. Fatigue **28**, 1752–1758 (2006)

67. Jiang, H.; Bowen, B.; Knott, J.F.: Fatigue performance of a cast aluminium alloy Al–7Si–Mg with surface defects. J. Mater. Sci. **34**, 719–725 (1999)

68. Ammar, H.R.; Samuel, A.M.; Samuel, F.H.: Effects of surface porosity on the fatigue strength of AE425 and PM390 hypereutectic Al–Si casting alloys at medium and elevated temperatures. Mater. Sci. Eng. A **473**, 58–64 (2008)

69. Liu, S.J.; Yang, G.Y.; Lou, S.F.; Jie, W.Q.: Microstructure and mechanical properties of sand mould cast Mg–4.58Zn–2.6Gd–0.18Zr magnesium alloy after different heat treatments. J. Alloys Compd. **644**, 846–853 (2015)

70. Hernandez, F.C.R.; Sokolowski, J.H.: Effects and on-line prediction of electromagnetic stirring on microstructure refinement of the 319 Al–Si hypoeutectic alloy. J. Alloys Compd. **480**, 416–421 (2009)

71. Lu, D.; Jiang, Y.; Guan, G.; Zhou, R.; Li, Z.; Zhou, R.: Refinement of primary Si in hypereutectic Al–Si alloy by electromagnetic stirring. J. Mater. Process. Technol. **189**, 13–18 (2007)

72. Jin, Y.X.; Hua, L.; Xu, X.; Peng, Q.: The effect of electromagnetic stirring on the microstructure and corrosion of mischmetal modified AZ91D magnesium alloy. Mater. Sci. **27**, 171–185 (2009)

73. Liu, S.F.; Liu, L.Y.; Kang, L.G.: Refinement role of electromagnetic stirring and strontium in AZ91 magnesium alloy. J. Alloys Compd. **450**, 546–550 (2008)

74. Girija, K.; Satyanarayana, I.: Improved mechanical properties and microstructure of mechanical vibration mould during solidification. Int. J. Adv. Res. Manag. Archit. Technol. Eng. **1**, 21–23 (2015)

75. Kumar, S.; Tewari, S.P.: Effect of vibration on mechanical properties of A356 aluminum alloy casting. Int. J. Mech. Prod. Eng. Res. Dev. **5**, 75–80 (2015)

76. Abu-Dheir, N.; Khraisheh, M.; Saito, K.; Male, A.: Silicon morphology modification in the eutectic Al–Si alloy using mechanical mould vibration. Mater. Sci. Eng. A **393**, 109–117 (2005)

77. Fouad, Y.; Batanouny, M.E.I.: Effect of surface treatment on wear behaviour of magnesium alloy AZ31. Alex. Eng. J. **50**, 19–22 (2011)

78. Campbell, F.: Manufacturing Technology for Aerospace Structural Materials, 1st edn. Elsevier, Amsterdam (2006)

79. Kainer, K.: Metal Matrix Composites. Custom-Made Materials for Automotive and Aerospace Engineering. Wiley, Hoboken, NJ (2006)

80. Fernández, H.; Ordonez, S.; Pesenti, H.; Gonzálezc, R.E.; Leoni, M.: Microstructure homogeneity of milled aluminum A356–Si_3N_4 metal matrix composite powders. J. Mater. Res. Technol. (2019). https://doi.org/10.1016/J.JMRT.2019.05.004

81. Roseline, S.; Paramasivam, V.: Corrosion behaviour of heat treated aluminium metal matrix composites reinforced with fused zirconia alumina 40S. J. Alloys Compd. (2019). https://doi.org/10.1016/j.jallcom.2019.05.185

82. Fayomi, J.; Popoola, A.P.I.; Oladijo, O.P.; Popoola, O.M.; Fayomi, O.S.I.: Experimental study of ZrB2-Si3N4 on the microstructure, mechanical and electrical properties of high grade AA8011 metal matrix composites. J. Alloys Compd. (2019). https://doi.org/10.1016/j.jallcom.2019.03.112

83. Mkpume, C.C.D.; Okonkwo, E.G.; Aigbodion, V.S.; Offor, P.O.; Nnakwo, K.C.: Silica sand modified aluminium composite: an empirical study of the physical, mechanical and morphological properties. Mater. Res. Express **6**, 076539 (2019)

84. Prasad, D.S.; Krishna, A.R.: Fabrication and characterization of A356.2-rice husk ash composite using stir casting technique. Int. J. Eng. Sci. Technol. **2**, 7603–7608 (2010)

85. Singh, H.; Sarabjit, N.J.; Tyagi, A.K.: An overview of metal matrix composite: processing and SiC based mechanical properties. J. Eng. Res. Stud. **2**, 72–78 (2011)